Lithos 132-133 (2012) 50–69

Contents lists available at SciVerse ScienceDirect

Lithos

journal homepage: www.elsevier.com/locate/lithos

Coexistence of abyssal and ultra-depleted SSZ type mantle peridotites in a Neo-Tethyan Ophiolite in SW Turkey: Constraints from mineral composition, whole-rock geochemistry (major–trace–REE–PGE), and Re–Os isotope systematics

İbrahim Uysal [a,*], E. Yalçın Ersoy [b], Orhan Karslı [c], Yildirim Dilek [d], M. Burhan Sadıklar [a], Chris J. Ottley [e], Massimo Tiepolo [f], Thomas Meisel [g]

[a] Department of Geological Engineering, Karadeniz Technical University, TR-61080 Trabzon, Turkey
[b] Department of Geological Engineering, Dokuz Eylül University, TR-35160 Izmir, Turkey
[c] Department of Geological Engineering, Gümüşhane University, TR-29000 Gümüşhane, Turkey
[d] Department of Geology & Environmental Earth Sciences, Miami University, Oxford, OH 45056, USA
[e] Northern Centre for Isotopic and Elemental Tracing, Department of Earth Sciences, University of Durham, DH1 3LE Durham, UK
[f] Dipartimento di Scienze della Tedrra, Universita di Pavia, Via Ferrata, 1-27100 Pavia, Italy
[g] Department of General and Analytical Chemistry, University of Leoben, A-8700 Leoben, Austria

ARTICLE INFO

Article history:
Received 5 January 2011
Accepted 10 November 2011
Available online 18 November 2011

Keywords:
Upper mantle peridotites
Neo-Tethyan ophiolites
Partial melting
Melt percolation and refertilization in the upper mantle
Re/Os isotope systematics of peridotites

ABSTRACT

We present new, whole-rock major and trace element chemistry, including rare earth elements (REE), platinum-group elements (PGE), and Re–Os isotope data from the upper mantle peridotites of a Cretaceous Neo-Tethyan ophiolite in the Muğla area in SW Turkey. We also report extensive mineral chemistry data for these peridotites in order to better constrain their petrogenesis and tectonic environment of formation. The Muğla peridotites consist mainly of cpx-harzburgite, depleted harzburgite, and dunite. Cpx-harzburgites are characterized by their higher average CaO (2.27 wt.%), Al_2O_3 (2.07 wt.%), REE (53 ppb), and $^{187}Os/^{188}Os_{(i)}$ ratios varying between 0.12497 and 0.12858. They contain Al-rich pyroxene with lower Cr content of coexisting spinel (Cr# = 13–22). In contrast, the depleted harzburgites and dunites are characterized by their lower average CaO (0.58 wt.%), Al_2O_3 (0.42 wt.%), and REE (1.24 ppb) values. Their clinopyroxenes are Al-poor and coexist with high-Cr spinel (Cr# = 33–83). The $^{187}Os/^{188}Os_{(i)}$ ratios are in the range of 0.12078–0.12588 and are more unradiogenic compared to those of the cpx-harzburgites.

Mineral chemistry and whole rock trace and PGE data indicate that formation of the Muğla peridotites cannot be explained by a single stage melting event; at least two-stages of melting and refertilization processes are needed to explain their geochemical characteristics. Trace element compositions of the cpx-harzburgites can be modeled by up to ~10–16% closed-system dynamic melting of a primitive mantle source, whereas those of the depleted harzburgites and dunites can be reproduced by ~10–16% open-system melting of an already depleted (~16%) mantle. These models indicate that the cpx-harzburgites are the products of first-stage melting and low-degrees of melt–rock interaction that occurred in a mid-ocean ridge (MOR) environment. However, the depleted harzburgites and dunites are the product of second-stage melting and related refertilization which took place in a supra subduction zone (SSZ) environment. The Re–Os isotope systematics of the Muğla peridotites gives model age clusters of ~250 Ma, ~400 Ma and ~750 Ma that may record major tectonic events associated with the geodynamic evolution of the Neo-Tethyan, Rheic, and Proto-Tethyan oceans, respectively. Furthermore, >1000 Ma model ages can be interpreted as a result of an ancient melting event before the Proto-Tethys evolution.

1. Introduction

On-land fragments of the ancient upper mantle peridotites provide critical and 3-dimensional information on the mode and nature of magmatic, tectonic, and geochemical processes controlling the evolution of the oceanic lithosphere (Dilek and Furnes, 2011). Geochemical and petrological data from ophiolitic and abyssal peridotites have presented new insights into our understanding of the compositional heterogeneity of the upper mantle that has been mainly induced by varying degrees of partial melting in earth history (Choi et al., 2008; Dilek and Morishita, 2009; Niu et al., 1997; Takazawa et al., 2000). However, the textures and mineral chemistry of some peridotites are inconsistent to be residual in origin and these peridotites are interpreted to be the product of impregnation with melt.

* Corresponding author. Tel.: +90 532 3024578; fax: +90 462 3257405.
E-mail addresses: iuysal@ktu.edu.tr, uysal.ibrahim@gmail.com (İ. Uysal).

0024-4937/$ – see front matter © 2011 Elsevier B.V. All rights reserved.
doi:10.1016/j.lithos.2011.11.009

Therefore, partial melting is considered not the only cause of mantle heterogeneity; melt–rock reaction processes can also produce significant chemical heterogeneity in the mantle (Aldanmaz et al., 2009; Bodinier et al., 2008; Choi et al., 2008; Hanghoj et al., 2010; Kelemen et al., 1992; Rampone et al., 2008; Uysal et al., 2007; Zhou et al., 2005). Furthermore, the effects of melt–rock percolation–reaction processes on Re–Os isotopic systems and platinum group elements (PGE) have been the focus of recent studies because of their significance in the upper mantle evolution (e.g. Acken et al., 2008; Alard et al., 2000, 2002; Batanova et al., 2008; Lorand and Alard, 2001; Luguet et al., 2003; Melcher and Meisel, 2004; Zhou et al., 2005). These authors also demonstrated that melt extraction is not the main control on Re abundances and $^{187}Os/^{188}Os$ of mantle peridotites and these values can be significantly affected by different styles of melt or fluid percolation in mantle. The compositions of the minerals in peridotites are also important recorders of the physical conditions of their post-subsolidus evolution and related processes in the upper mantle. Detailed and systematic studies of chemical and mineralogical variations of the upper mantle peridotites are, however, surprisingly limited in present time (e.g., Bodinier and Godard, 2003 and references therein; Acken et al., 2008; Aldanmaz et al., 2009; Batanova et al., 2008; Godard et al., 2008;).

Ophiolitic peridotites are by far the most important source of structural, petrological and geochemical information on the chemical make-up of the upper mantle. The majority of the studies on ophiolites around the world have focused on mainly the petrology and geochemistry of their crustal units, while most of the studies in the ophiolitic peridotites have mainly emphasized asthenospheric and lithospheric deformation patterns and their spatial and temporal relationships in them (see Dilek et al., 2000, and the papers therein). Hence, well preserved and relatively fresh peridotite rocks in ophiolites, whose regional tectonic evolution is well understood through field-based interdisciplinary studies, are the best natural laboratories to investigate the chemical geodynamics of ancient upper mantle.

In a recent pilot study of a small section of the upper mantle peridotites in the Cretaceous Muğla ophiolite in SW Turkey (Ortaca, Muğla), we demonstrated their compositionally heterogeneous nature and the occurrence of Al- and Cr-rich chromitites with variable Os-isotopic compositions in them (Uysal et al., 2005, 2007, 2009). In this current study we undertook a more detailed and systematic geochemical and isotopic investigation of these ophiolitic peridotites in order to better constrain their melt evolution and chemical geodynamics. To this end, we present here new mineral chemical, whole-rock major and trace–rare earth element abundances, as well as PGE and Re–Os isotopic data, and examine the tectonic evolution of the Muğla ophiolite from the perspective of its upper mantle evolution.

2. Geological setting

Two major ophiolite belts occur in the Eastern Mediterranean region: (1) the Jurassic and possibly older ophiolites of the Dinarides–Hellenides mountain belt in the Balkan Peninsula, and in northern Anatolia (Dilek and Furnes, 2009; Dilek and Thy, 2006; Robertson, 2002) and (2) the E–W-trending Cretaceous ophiolites of the Tauride mountain belt in southern Anatolia–Turkey (Dilek et al., 1999) and southern Iran (Ghazi et al., 2010 and references therein). The ophiolites in SW Anatolia form the westernmost part of the ophiolite belts of the Taurides, and have been widely interpreted to have originated from a Tethyan suture zone between the Sakarya and Anatolide–Tauride continental blocks in the north (Fig. 1a). The upper mantle peridotites in the Muğla area (Fig. 1b) are part of this western Taurides ophiolite belt, and contain abundant chromite deposits. They were dated by K–Ar method at 88 ± 4 to 102 ± 4 Ma (Thuizat et al., 1981). The Tauride ophiolites represent fragments of a suprasubduction zone oceanic lithosphere resting tectonically on the platform carbonates of the Taurides (e.g. Dilek et al., 1999; Robertson, 2002; Uysal, 2007; Uysal et al., 2007).

The western Taurides can be subdivided into three main geological units: the Beydağlari autochthon, comprising a thick platform of shallow-marine carbonates of Liassic to Lower Miocene age with an unknown crustal basement; the Antalya nappe, emplaced westwards in Late Cretaceous time; and the younger Lycian nappe complex emplaced towards the southeast (Fig. 1b). The Antalya nappe is an assemblage of Mesozoic sedimentary, igneous and metamorphic rocks, including ophiolites and parautochthonous carbonates, which were thrust onto the autochthon from the east during the closure of the north-trending southern Neotethys branch (Dilek and Rowland, 1993; Poisson et al., 2003). The Lycian nappes, which are composed of tectonostratigraphic units developed in different environmental conditions, owe their origin to the early Tertiary closure of a Neotethys branch along the İzmir–Ankara suture zone, between the Menderes microcontinent accreted earlier to the north and the Beydağlari microcontinent advancing from the south (Okay et al., 2001). One of these units, i.e. mantle tectonites of the Muğla ophiolites, contains abundant chromite deposits which are economically important and actively being mined. This younger nappe complex was emplaced in the latest Cretaceous to early Tertiary, and was interpreted to represent a north-facing Mesozoic rift and passive margin of the İzmir–Ankara Neotethys branch (Collins and Robertson, 2003). The tectonic loading of the autochthon by the Lycian nappes resulted in the development of a peripheral foreland basin to the southeast of the nappe front. The readers are referred to Okay et al. (2001) and Robertson (2002) for further details.

3. Field occurrence and petrography of the Muğla peridotites

For this study we collected forty-five samples from the major lithologies (Fig. 1c). The upper mantle peridotites in the Muğla area consist mainly of cpx-harzburgite (~25%), harzburgite (~60%), and dunite (~15%) based on modal mineralogy, whole-rock, and mineral compositions (Table 1). The main body of these peridotites shows m- to 100-m-scale heterogeneity, with no systematic distribution, in terms of its modal mineralogy, Cr# [$100Cr/(Cr+Al) = 13–83$] in spinel, and bulk composition (Fig. 1c). However, the clinopyroxene (cpx)-rich harzburgites appear to be more abundant in the northwestern part of the study area. The rocks are cut by abundant magnesite veinlets and pervasively foliated. Randomly oriented, 1- to 2-m-thick dolerite and up to 20-cm-thick pyroxenite dikes intrude the peridotites. The contacts between the depleted harzburgite and cpx-harzburgite are transitional at the cm- to meter-scale and cannot be mapped in the field. Gabbros and other cumulate rocks are absent in the Muğla ophiolites.

The cpx-harzburgite rock unit consists mainly of ol (66–78%), opx (17–28%), cpx (4–5%), and spl (<2%) (see Table 1 for mineral abbreviations). Depleted harzburgites displaying porphyroblastic and granoblastic textures contain ol (66–89%), opx (9–32%) and cpx (<3.6%). Elongated and deformed spinel grains occupy up to 1.8% of the thin-section areas in the studied samples. Dunite occurs as channels and lenses (up to few 10s of meter) within the harzburgites, and also form an envelope (up to few centimeters to decimeters) around the chromitite bodies of various sizes. Dunitic rocks contains ol (92–99%), opx (<7%), spl (<2%), and cpx (<1%) (Table 1).

The majority of the samples we investigated are overprinted to varying degrees by the growth of serpentine minerals, which can

Fig. 1. (a) Distributions of the major ophiolite complexes on a map showing the major blocks of Turkey. NAFZ: North Anatolian Fault Zone, EAFZ: East Anatolian Fault Zone; (b) Simplified geological map of south-western Turkey (after Alçiçek, 2007; Şenel, 1997); (c) Sampling location of peridotite samples. Symbols used in all figures are as follows: square for cpx-harzburgite, circle for depleted harzburgite and triangle for dunite.

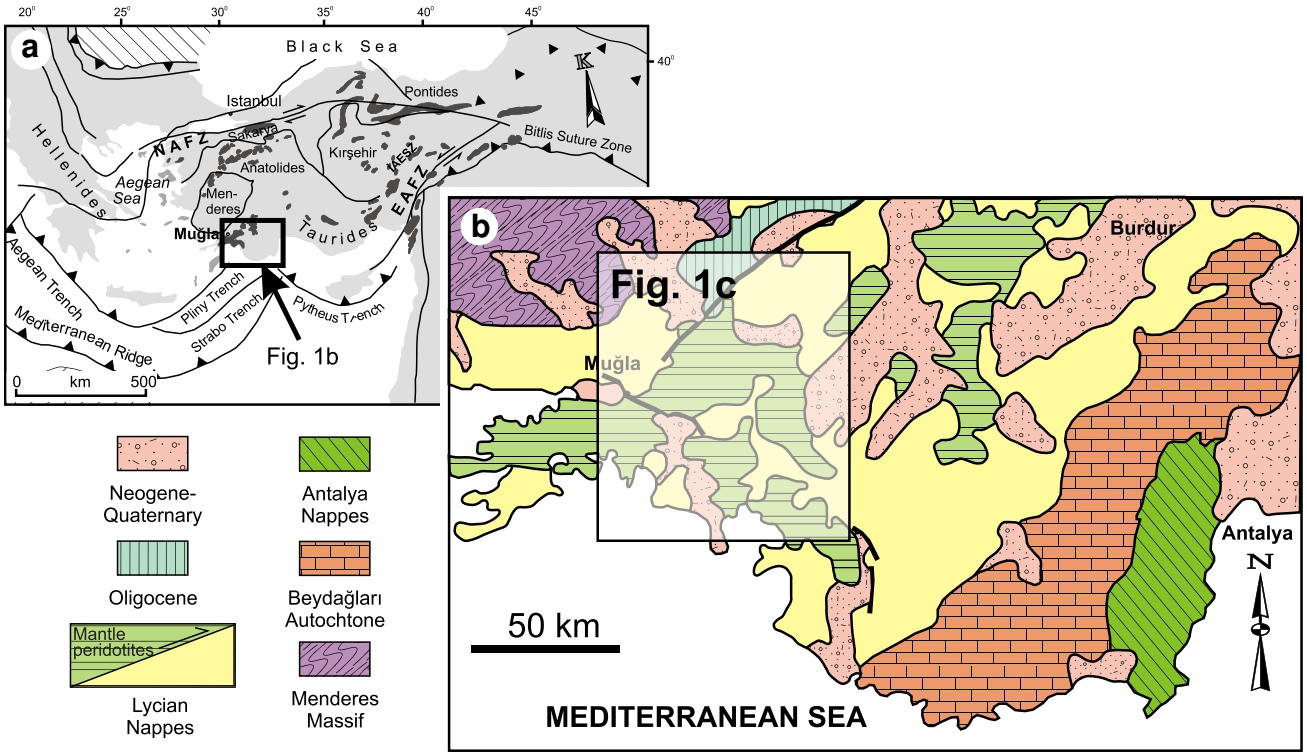
a
Black Sea
Istanbul
Pontides
Sakarya
Kırşehir
Bitlis Suture Zone
NAFZ
KESZ
EAFZ
Hellenides
Aegean Sea
Anatolides
Men-deres
Taurides
Muğla
Aegean Trench
Pliny Trench
Strabo Trench
Pytheus Trench
Mediterranean Ridge
Fig. 1b
0 km 500
b
Fig. 1c
Muğla
Burdur
Antalya
50 km
MEDITERRANEAN SEA
Neogene-Quaternary
Oligocene
Mantle peridotites
Lycian Nappes
Antalya Nappes
Beydağları Autochtone
Menderes Massif

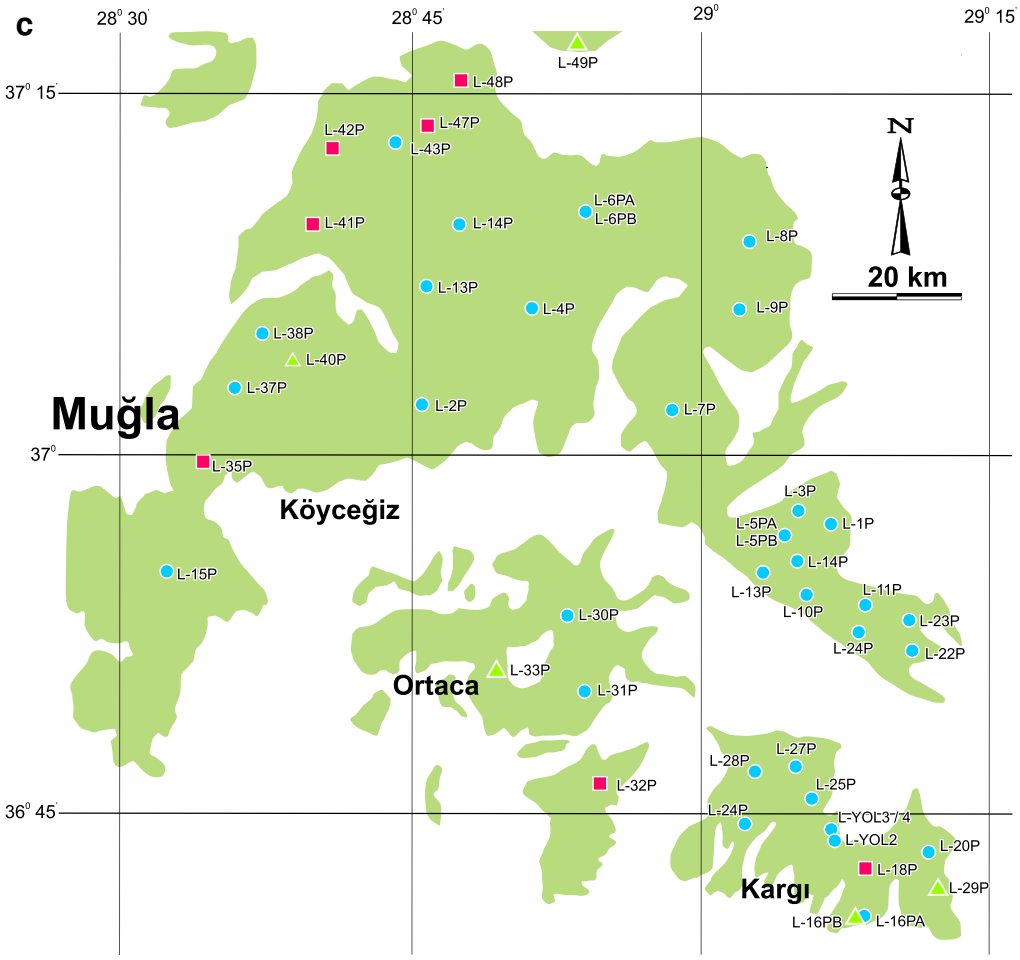
c
28° 30'
28° 45'
29°
29° 15'
37° 15'
37°
36° 45'
L-49P
L-48P
L-47P
L-42P
L-43P
L-41P
L-14P
L-6PA
L-6PB
L-8P
L-13P
L-4P
L-9P
L-38P
L-40P
L-37P
L-2P
L-7P
L-35P
Muğla
Köyceğiz
L-15P
L-3P
L-5PA
L-5PB
L-1P
L-14P
L-13P
L-11P
L-10P
L-23P
L-24P
L-22P
L-30P
L-33P
Ortaca
L-31P
L-32P
L-27P
L-28P
L-25P
L-24P
L-YOL3-4
L-YOL2
L-20P
L-18P
L-29P
Kargı
L-16PB
L-16PA
N
20 km

Table 1
Classification of peridotite samples as clinopyroxene rich harzburgite (cpx-harzburgite), depleted harzburgite and dunite, on the basis of modal abundance of minerals, whole-rock geochemistry and composition of the minerals in peridotites. Ol: olivine, Opx: orthopyroxene, Cpx: clinopyroxene, Spl: spinel, σ: standard deviation, Fo = 100 Mg/(Mg + Fe^{2+}); Cr# = 100Cr/(Cr + Al).

						Ol		Opx						Cpx						Spl			
		Ol (%)	Opx (%)	Cpx (%)	Spl (%)	Fo (%)	σ	Al_2O_3 (wt.%)	σ	En (%)	σ	Mg#	σ	Al_2O_3 (wt.%)	σ	Di (%)	σ	Mg#	σ	Cr#	σ	Mg#	σ
Cpx-harzburgite	L18P	70.2	23.5	4.7	1.6	90.0	0.2	3.80	0.4	88.4	1.0	90.0	0.5	4.09	0.6	47.1	1.5	92.8	0.5	20.9	0.4	71.6	0.6
	L32P	77.9	16.6	4.0	1.5	90.1	0.2	4.12	0.4	89.0	0.5	90.3	0.2	5.57	0.8	49.0	1.4	92.5	0.5	17.9	1.4	72.6	7.1
	L35P	74.3	19.0	5.0	1.7	90.6	0.3	4.62	1.1	88.9	1.9	90.7	0.4	4.47	0.7	47.7	3.1	92.8	0.8	16.2	0.5	76.3	0.6
	L41P	75.5	18.2	4.4	1.9	–	–	–	–	–	–	–	–	–	–	–	–	–	–	–	–	74.8	1.5
	L42P	73.6	19.9	4.9	1.6	90.5	0.1	5.21	0.8	87.1	1.5	90.3	0.3	5.62	0.8	48.9	1.7	92.8	0.6	15.2	2.5	72.3	1.1
	L47P	74.3	20.1	3.9	1.7	90.0	0.1	4.59	0.0	88.6	0.1	90.4	0.2	3.57	0.5	47.5	1.4	93.0	0.7	18.6	0.7	74.0	1.7
	L48P	65.8	27.9	4.8	1.5	89.8	0.1	4.36	0.7	88.1	1.0	89.9	0.3	4.78	0.5	48.7	1.4	92.6	0.6	17.5	0.8	55.6	0.5
Harzburgite	L1PA	78.7	18.7	0.9	1.7	91.6	0.4	1.59	0.1	89.4	0.8	91.4	0.19	0.64	–	46.5	–	95.0	–	58.8	0.9	55.6	0.5
	L2P	77.3	19.5	1.7	1.5	–	–	–	–	–	–	–	–	–	–	–	–	–	–	–	–	–	–
	L4P	75.5	21.3	1.4	1.8	–	–	–	–	–	–	–	–	–	–	–	–	–	–	–	–	–	–
	L5PA	83.4	15.1	0	1.5	91.8	0.3	1.10	0.0	–	–	–	–	–	–	–	–	–	–	64.0	1.2	52.5	1.3
	L5PB	81.0	17.3	0	1.7	91.5	0.4	1.09	0.0	–	–	–	–	–	–	–	–	–	–	54.7	2.9	49.0	7.7
	L6PA	79.0	18.1	1.5	1.4	–	–	–	–	–	–	–	–	–	–	–	–	–	–	–	–	–	–
	L6PB	73.6	23.5	1.2	1.7	91.5	0.2	1.95	0.2	–	–	–	–	1.10	0.1	–	–	–	–	52.2	0.9	57.7	0.5
	L7P	77.6	19.4	1.5	1.5	–	–	–	–	–	–	–	–	–	–	–	–	–	–	–	–	–	–
	L8P	80.6	16.5	1.3	1.6	–	–	–	–	–	–	–	–	–	–	–	–	–	–	–	–	–	–
	L9P	75.0	21.7	1.7	1.6	–	–	–	–	–	–	–	–	–	–	–	–	–	–	–	–	–	–
	L10P	71.8	23.5	3.0	1.7	91.3	0.2	2.14	0.2	89.6	1.0	91.6	0.3	1.12	0.1	48.1	0.1	95.2	0.1	53.1	1.5	61.5	1.2
	L11P	77.4	19.4	1.8	1.4	91.2	0.3	1.56	0.1	89.6	2.5	91.6	0.2	1.70	0.2	46.5	1.2	94.4	0.3	59.3	2.0	54.6	1.1
	L13P	72.9	24.0	1.5	1.6	–	–	–	–	–	–	–	–	–	–								
	L14P	77.9	17.3	3.1	1.7	91.2	0.3	2.24	0.2	89.2	4.9	91.3	0.3	2.91	0.2	48.9	0.5	93.8	0.3	46.1	3.0	61.2	1.3
	L15P	77.6	18.0	2.6	1.8	91.4	0.6	1.91	0.2	90.0	0.5	91.3	0.2	2.20	0.3	48.1	1.4	94.0	0.4	51.4	1.6	57.2	1.2
	L16PA	82.0	16.1	0.2	1.7	92.1	0.4	1.36	0.3	89.5	2.3	91.3	0.2	1.09	0.1	46.7	0.8	95.1	0.1	52.7	0.6	58.9	0.5
	L22P	82.5	14.5	1.3	1.7	92.1	0.3	–	–	–	–	–	–	–	–	–	–	–	–	–	–	–	–
	L23P	78.8	18.0	1.6	1.6	–	–	–	–	–	–	–	–	–	–	–	–	–	–	–	–	–	–
	L24P	70.3	26.0	2.0	1.7	–	–	–	–	–	–	–	–	–	–	–	–	–	–	–	–	–	–
	L25P	77.4	20.0	0.9	1.7	–	–	–	–	–	–	–	–	–	–	–	–	–	–	–	–	–	–
	L27P	73.3	23.7	1.5	1.5	–	–	–	–	–	–	–	–	–	–	–	–	–	–	–	–	–	–
	L28P	86.0	11.7	0.8	1.5	–	–	–	–	–	–	–	–	–	–	–	–	–	–	–	–	–	–
	L30P	80.2	18.1	0	1.7	92.0	0.1	1.92	0.0	88.7	1.3	91.5	0.1	–	–	–	–	–	–	56.6	0.9	55.8	0.3
	L31P	77.0	20.2	1.2	1.6	–	–	–	–	–	–	–	–	–	–	–	–	–	–	–	–	–	–
	L37P	85.9	11.7	0.8	1.6	–	–	–	–	–	–	–	–	–	–	–	–	–	–	–	–	–	–
	L38P	78.0	16.8	3.6	1.6	90.8	0.2	2.71	0.2	90.8	0.46	90.8	0.5	3.39	0.7	48.0	1.3	94.0	0.6	37.6	1.0	65.1	0.6
	L43P	66.4	32.0	0	1.6	–	–	–	–	–	–	–	–	–	–	–	–	–	–	–	–	–	–
	LYOL2	89.2	8.8	0	2.0	92.6	0.2	–	–	–	–	–	–	–	–	–	–	–	–	76.2	0.3	48.0	0.6
	LYOL3	76.9	21.5	0	1.6	92.4	0.6	1.63	0.1	90.3	0.4	91.8	0.16	–	–	–	–	–	–	58.3	2.7	57.5	1.4
	LYOL4	78.5	19.5	0.5	1.5	–	–	–	–	–	–	–	–	–	–	–	–	–	–	–	–	–	–
	LYOL5	80.4	17.3	0.8	1.5	–	–	–	–	–	–	–	–	–	–	–	–	–	–	–	–	–	–
	L3P	88.1	9.6	0.8	1.5	91.5	0.4	1.16	0.1	89.8	0.9	91.6	0.2	0.98	0.2	48.0	0.7	95.2	0.3	66.4	1.5	50.8	1.1
	L20P	87.4	10.5	0.6	1.5	92.0	0.2	0.98	0.2	91.7	0.4	92.8	0.3	–	–	–	–	–	–	73.4	0.8	42.8	1.3
Dunite	L16PB	91.8	6.6	0.4	1.2	92.2	0.4	–	–	–	–	–	–	–	–	–	–	–	–	74.8	0.2	46.0	0.4
	L29P	97.2	0.8	0.5	1.5	–	–	–	–	–	–	–	–	–	–	–	–	–	–	–	–	–	–
	L33P	98.5	0	0	1.5	–	–	–	–	–	–	–	–	–	–	–	–	–	–	–	–	–	–
	L40P	96.2	2.0	0.4	1.4	–	–	–	–	–	–	–	–	–	–	–	–	–	–	–	–	–	–
	L49P	98.3	0	0.2	1.5	92.8	0.3	–	–	–	–	–	–	–	–	–	–	–	–	81.4	0.3	41.5	1.8

reach up to 92% of the total surface area in some samples. Despite the high degree of serpentinization of these samples, it was possible to distinguish relicts of primary olivine grains. Although the spinel-group minerals are less affected by the secondary processes, the spinel grains in harzburgites stand out as more extensively altered than those of dunite and chromitites. Ferrian chromite and magnetite, the alteration product of spinels, occur along the rims of spinel grains. In these cases, we used the unaltered cores of the spinel grains for petrogenetic interpretations.

Olivine commonly forms elongated porphyroblasts that are up to 5 mm in diameter and mostly smaller (1–2 mm in diameter). Olivine neoblasts (<0.5 mm in diameter) also occur around the larger olivine and orthopyroxene grains (Fig. 2a, b).

Orthopyroxene grains are commonly seen as porphyroblasts, approximately 7–8 mm in length, and are generally unaltered (Fig. 2a, b). Large orthopyroxene grains are surrounded by anhedral and small olivine crystals (Fig. 2a), and show clinopyroxene lamellae (Fig. 2d, e).

Textural and chemical compositions of clinopyroxene provide significant information on the petrology of peridotites even though its modal abundance is very low in these rocks. The analyzed samples contain two types of clinopyroxenes: (1) primary clinopyroxene porphyroblasts with irregular rims that are residual after partial melting

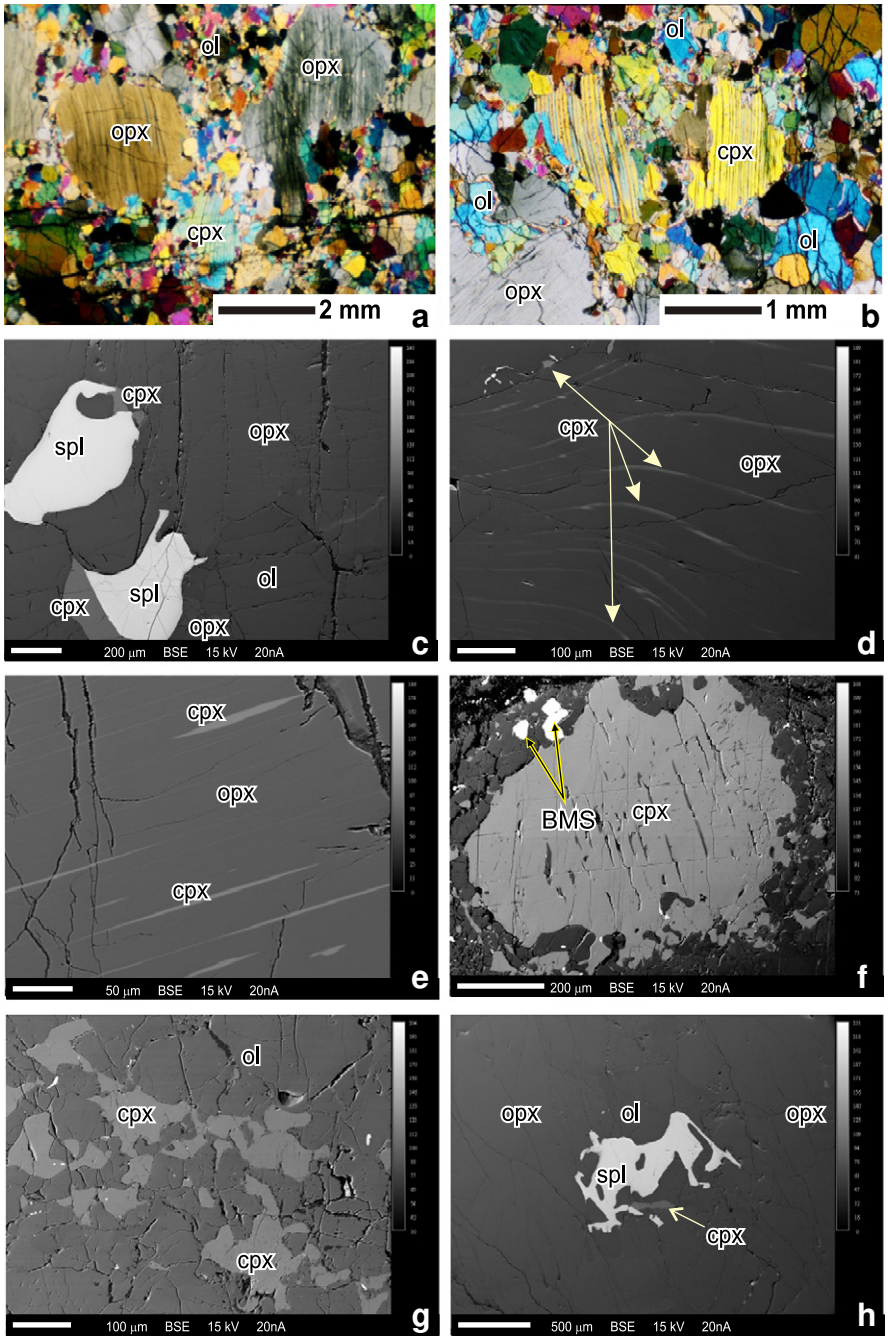

Fig. 2. (a–b) thin section images of peridotite samples showing the porphyroblastic textures (crossed nicol); (c–h) back scattered electron (BSE) images from the polished thin sections of peridotite samples. (c) Association of anhedral spinel and clinopyroxene with olivine and orthopyroxene porphyroblasts. Exsolution lamellae of clinopyroxene in deformed (d) and undeformed (e) orthopyroxene. (f) Primary clinopyroxene porphyroblasts in cpx-harzburgite coexisting with small base metal sulfide (BMS) grains. The exsolutions lamellae in clinopyroxene and the reaction corona around the clinopyroxene is orthopyroxene. (g) Blocky intergranular clinopyroxene associated with olivine. (h) Anhedral spinel grain coexisting with small clinopyroxene and, olivine and orthopyroxene porphyroblasts in harzburgite. ol: olivine, opx: orthopyroxene, cpx: clinopyroxene, spl: spinel, BMS: base metal sulfide.

(Fig. 2f), and (2) secondary clinopyroxene that commonly occurs as an interstitial phase along grain boundaries with olivine in some of the depleted harzburgite samples (Fig. 2g); this type represents melt impregnation artifacts in previously depleted peridotites (the samples L20P, LYOL2, L3P, L10P, L15P) (cf., Alard et al., 2005; Luguet et al., 2001; Nicolas and Prinzhofer, 1983; Seyler et al., 2001).

Spinel (1.5–2 vol.%), found in all samples was affected by lithospheric deformation in the harzburgites, resulting in elongated grain shapes (Fig. 2c, h). Euhedral spinel crystals occur in dunitic samples as a result of the reaction between percolating basaltic melt and the tectonites. In highly altered samples, some spinels were altered to ferrian chromite or completely changed to magnetite.

Base metal sulfides (BMS) have been observed in especially cpx-rich harzburgite (Fig. 2f), although a few grains have also been detected in the depleted harzburgites. Most of the BMS grains display partial replacement of the primary sulfide phases.

4. Analytical techniques

Mineral compositions were determined using a Cameca SX-100 electron microprobe at the Institute of Mineralogy and Petrology in Hamburg (Germany), equipped with five wavelength-dispersive spectrometers and an energy-dispersive Pentafet semiconductor Si–Li system. Analytical conditions are 15 kV accelerating voltage, 20 nA beam current and 10 to 30 s counting time for silicates (30 s for Al, Ni, Ca; 20 s for Ti and 10 s for all other elements). For the spinel, counting times of 100 s for Ti, 30 s for Ni, and 10 s for all other elements were employed, with a beam diameter of 1 μm. For calibration, natural and synthetic standards were used. Raw data were revised by a PAP (Pouchou and Pichoir, 1984) matrix correction. Detection limits of the oxides are given in Appendix 1.

Whole-rock samples were analyzed by X-ray fluorescence at the University of Hamburg (Germany) for major elements. Concentration of the REE (Rare Earth Elements) and some trace elements (Rb, Sr, Y, Zr, Cs, Ba, Hf, Nb, Ta, U, and Th) were determined by Inductively Coupled Plasma Mass Spectroscopy (ICP-MS) using a Thermo Scientific X-Series2 in the Department of Earth Sciences at the University of Durham, following a standard nitric and hydrofluoric acid digestion (Ottley et al., 2003). Sample preparation work was undertaken in clean air laminar flow hoods. Briefly the procedure is as follows; into a Teflon vial 4 ml HF and 1 ml HNO_3 (SPA, ROMIL Cambridge) is added to 100 mg of powdered sample, the vial is sealed and left on a hot plate at 150 °C for 48 h. The acid mixture was evaporated to near dryness, the moist residue has 1 ml HNO_3 added and was evaporated again to near dryness. A second 1 ml HNO_3 was again added and evaporated to near dryness these steps convert insoluble fluoride species into soluble nitrate species. Finally 2.5 ml HNO_3 was added and diluted to 50 ml after the addition of an internal standard giving a final concentration of 20 ppb Re and Rh. The internal standard was used to compensate for any analytical drift and matrix suppression effects. Calibration of the ICP-MS was via international rock standards (BHVO-1, AGV-1, W-2, NBS688) with the addition of an in-house peridotite standard (GP13) (Ottley et al., 2003). These standards and analytical blanks were prepared by the same technique as the samples. To improve the signal to noise threshold for the low abundance isotopes, instrument dwell times were increased (Ottley et al., 2003). The composition of the reference samples (W-2, AGV-1, BHVO-1, BE-N, NBS688) was analyzed as an unknown during the same analytical runs as Muğla samples. For the analyzed elements, reproducibility of these references samples is generally better than 2% and the measured composition compares favorably with that published information in Potts et al. (1992). Detection limits of each element, average blank values as well as average, standard

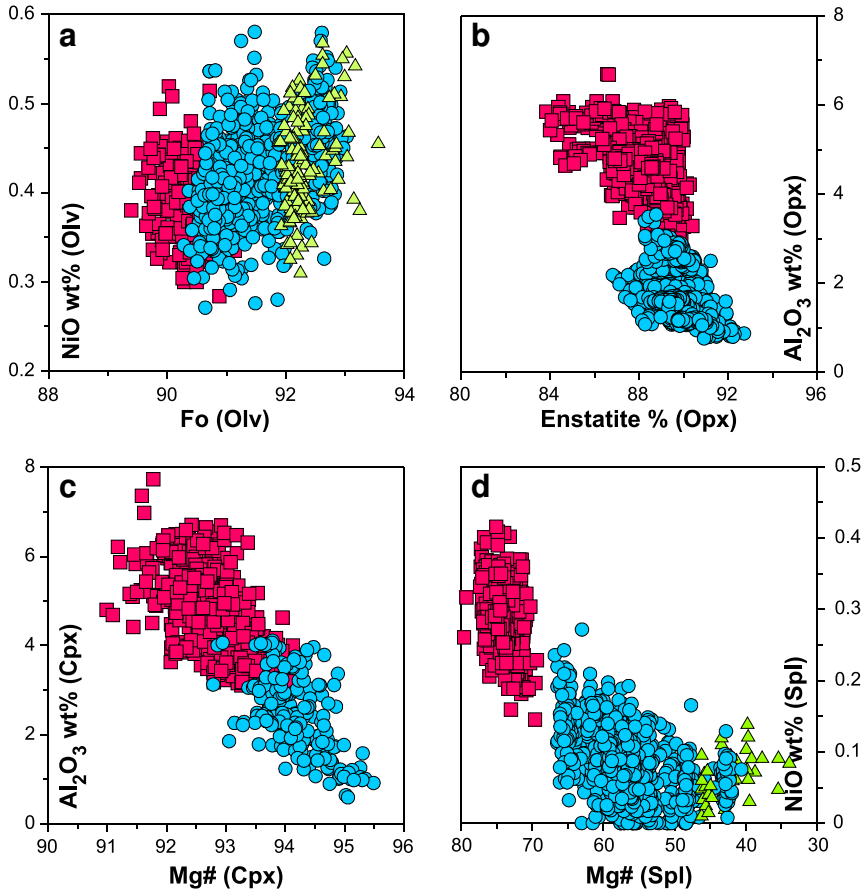

Fig. 3. Compositional variations of olivine (Fo vs. NiO wt.%) (a), orthopyroxene (En% vs. Al_2O_3 wt.%) (b), clinopyroxene (Mg# vs. Al_2O_3 wt.%) (c), and spinel phases (Mg# vs. NiO wt.%) (d) from the Muğla peridotites. Fo = 100 Mg/(Mg + Fe^{2+}) of olivine, En = 100 Mg/(Ca + Mg + Fe^{2+}) of orthopyroxene, and Mg# = 100 Mg/(Mg + Fe^{2+}) for clinopyroxene and spinel.

deviations and RSD% values of in-house peridotite standard (GP13) are included in Appendix 2.

Selected samples were analyzed for all PGE using a nickel sulfide fire-assay pre-concentration method followed by ICP-MS at Genalysis Laboratory, Perth, Western Australia. The detailed analytical procedure is already published in Gervilla et al. (2005). Rhenium and PGE concentrations of selected peridotite samples of varying lithologies were obtained on the same sample test solution by isotope dilution ICP-MS at the Montanuniversität Leoben, Austria, following the technique described by Meisel et al. (2003) and Paliulionyte et al. (2006).

Trace elements concentrations of primary clinopyroxenes, located on polished thin sections of 80 μm thickness, were determined by LAM–ICP-MS in Pavia, Italy. The instrument at the CNR–IGG of Pavia is a quadrupole ICP-MS (ELAN Drc-e; Perkin Elmer) coupled with a Q-switched Nd:YAG laser source (Quantel Brilliant), whose fundamental emission in the near-IR region (1064 nm) is converted to 266 nm by two harmonic generators (see Tiepolo et al., 2003 for details). Helium was used as a carrier gas and mixed with Ar downstream of the ablation cell. NIST 612 reference glass was used as an external standard and ^{43}Ca as internal standard. Precision and accuracy (<10% and <5%, respectively) were assessed on the USGS BCR-2g reference glass.

5. Compositions of mineral phases

5.1. Major oxide and trace element compositions

5.1.1. Olivine

Average olivine compositions and standard deviations for the investigated samples are given in Appendix 1a. The olivine composition is dependent on the rock lithology. The Fo content of the olivines decreases from dunite through harzburgite and cpx-harzburgite, although olivine in some harzburgite samples is represented by higher Fo content than those in dunite. Olivine in the harzburgites displays slight compositional differences, with Fo values of 90.3–92.9 and Ni content of 0.27–0.58 wt.%. Fo values for olivines in the cpx-harzburgites (Fo = 89.4–91.2) are lower but NiO contents are similar (0.28–0.52 wt.%), compared to those in the depleted harzburgites. Fo values of olivine from dunite range between 91.9 and 92.6 and Ni contents vary between 0.43 and 0.47 wt.% NiO (Fig. 3a).

5.1.2. Orthopyroxene

Orthopyroxene average chemical compositions and standard deviations are given in Appendix 1b. They have embedded rims and have been observed as subhedral to anhedral porphyroblasts. In some samples, large orthopyroxenes display thin exsolution lamellae of clinopyroxene (Fig. 2d and e). In highly altered samples, orthopyroxene may be replaced by serpentine forming bastite. The variations in the chemical composition of the orthopyroxene depend on the modal mineralogy of the peridotites. The enstatite (En) contents of orthopyroxenes in the depleted harzburgites range from 86.3 to 92.8, whereas they vary from 82.4 to 91.2 in the cpx-harzburgite (Fig. 3b). Hence, the En content of orthopyroxene correlates positively with increasing depletion of the peridotites. The Al_2O_3 content of orthopyroxene is variable and lies in the range of 3.08–6.68 wt.% in the cpx-harzburgite and 0.95–3.54 wt.% in the depleted harzburgites. This range shows a negative correlation with the En content (Fig. 3b).

5.1.3. Clinopyroxene

Average chemical compositions and standard deviations of residual clinopyroxenes are given in Appendix 1c. The residual clinopyroxenes are generally diopside in composition. The Mg# values of clinopyroxene in the cpx-harzburgite range from 91.0 to 94.9, and are lower than those for the depleted harzburgites (92.8–95.5). In addition, the Mg# correlates positively with the extent of depletion. The

Table 2
Trace and REE geochemistry (ppm) of primary clinopyroxenes from selected Muğla peridotite samples. –: Below detection limit (see Appendix 1d for detection limits).

Sample	L47P-4a	L47P-4b	L47P-6c	L18P-1r	L18P-1c	L38p-1a	L38P-2b	L38P-2c	L1PA-1d	L3P-2e
Rock-type	Cpx-H	Cpx-H	Cpx-H	Cpx-H	Cpx-H	H	H	H	H	H
Cs	0.004	0.002	–	0.016	0.015	–	0.003	–	–	0.14
Rb	–	0.039	0.051	0.083	0.054	0.040	0.081	0.079	–	7.360
Ba	0.101	0.119	0.100	0.260	0.147	0.050	–	0.048	0.032	50.59
Th	–	–	0.003	0.007	–	–	–	–	–	0.087
U	–	–	–	–	0.003	–	–	–	0.003	0.070
Nb	0.008	–	0.008	–	–	0.009	–	0.009	–	0.109
Ta	–	–	–	–	–	–	–	0.004	–	0.019
La	–	0.004	–	0.018	–	–	–	–	0.005	0.348
Ce	0.008	0.016	–	0.009	–	–	–	0.010	0.036	0.644
Pb	0.233	0.197	0.219	0.157	0.096	–	0.076	0.288	0.074	3.33
Pr	–	0.005	–	–	–	0.003	–	0.005	–	0.079
Sr	0.364	0.325	0.297	0.042	0.021	0.041	0.069	0.075	0.317	8.730
Nd	0.147	0.136	0.121	0.023	0.02	0.034	0.028	0.026	0.045	0.490
Zr	0.207	0.290	0.191	0.098	0.067	–	–	0.043	0.020	20.260
Hf	–	0.136	0.064	0.018	0.036	–	–	0.031	0.022	0.600
Sm	0.189	0.284	0.232	0.097	0.049	0.044	–	–	–	0.064
Eu	0.113	0.106	0.135	0.081	0.020	0.030	0.023	0.023	–	–
Gd	0.546	0.730	0.709	0.372	0.342	0.135	0.077	0.096	0.029	–
Ti	917	880	1298	863	797	457	480	416	138	114
Tb	0.125	0.145	0.173	0.098	0.073	0.048	0.074	0.064	0.008	0.027
Dy	1.289	1.570	1.520	0.788	0.683	0.489	0.623	0.678	0.054	0.053
Y	7.53	7.21	9.04	5.76	6.07	3.87	3.69	3.32	0.72	0.83
Ho	0.286	0.294	0.443	0.182	0.173	0.131	0.161	0.103	0.0265	0.016
Er	1.011	0.967	1.097	0.953	0.675	0.554	0.525	0.491	0.095	0.070
Tm	0.160	0.127	0.164	0.127	0.113	0.103	0.052	0.086	0.019	–
Yb	0.822	0.791	1.210	0.666	1.008	0.548	0.489	0.621	0.215	0.100
Lu	0.119	0.113	0.155	0.077	0.132	0.104	0.080	0.092	0.027	0.046
Sc	58.8	54.5	58.7	52.8	49.6	50.9	53.4	51.1	53.1	52.7
Cr	5081	5045	7203	6785	6505	8651	8478	7812	5058	3457
Ni	290	281	300	328	314	334	311	319	294	286
Co	19.4	17.7	19.1	19.5	17.8	19.6	23.2	21.7	18.5	21.0
V	219	211	246	255	240	224	227	218	174	126
Zn	8.31	4.10	9.86	6.61	5.72	10.73	8.66	8.93	7.05	9.84

clinopyroxene found in the less depleted cpx-harzburgite is characterized by a high Al_2O_3 content (3.01–7.72 wt.%) and low Mg# values. The clinopyroxene in harzburgites has a lower Al_2O_3 content (0.64–4.10 wt.%) and higher Mg# values (Fig. 3c). The TiO_2 content of clinopyroxene correlates negatively with Mg#, and it is higher in cpx-harzburgite (0.07–0.32 wt.%) than in the depleted harzburgite (<0.12 wt.%). The Na_2O content of clinopyroxenes in the cpx-harzburgite is in the range of 0.09–0.67 wt.%, higher than those in the depleted harzburgite (<0.29 wt.%). Secondary clinopyroxenes and exsolution lamellae in orthopyroxene crystals are diopside–endiopside in composition, and some grains display slight enrichment in Ti (<0.37 wt.% TiO_2) and Al (<6.04 wt.% Al_2O_3).

Selected trace element and REE compositions of the clinopyroxenes from the cpx-harzburgites and depleted harzburgites are given in Table 2 and whole data set is given in Appendix 1d. Trace element patterns of the clinopyroxene in the cpx-harzburgite resemble those of the clinopyroxenes from the abyssal peridotites (Fig. 4a and b). On the other hand, clinopyroxene in the harzburgites is more depleted in HREE and HFSE with respect to those of the abyssal peridotites and cpx-harzburgites. All clinopyroxene samples are characterized by strong enrichments in LILE and show negative Zr and Sr and positive Pb anomalies.

5.1.4. Spinel

Spinels in cpx-harzburgites, depleted harzburgites, and dunites are classified as *spinel*, *spinel to Mg-chromite*, and *Mg-chromite to chromite*, respectively, on the basis of their Cr# and Mg# values (not shown). However, to avoid misunderstanding, we use the term *spinel* for all the rock types in this study. Spinels in mantle peridotites are rarely affected by secondary processes. In the highly serpentinized samples, spinels have oxidized rims; therefore, only fresh cores were analyzed for this study. Spinel compositions and standard deviations are given in Appendix 1e. In contrast to other mafic silicates, the spinel analyzed in all the samples spans a wide compositional range due to the rock lithologies. The Cr# is lower in the cpx-harzburgite (13.4–22.2) than in the depleted harzburgite (32.5–77.2) or dunite (73.1–83.0); the cpx-harzburgite contains spinel of a higher Mg# (69.2–79.5) than the depleted harzburgite (41.1–67.8) or dunites (34.8–47.6). The NiO contents show a systematic decrease from cpx-harzburgites to dunites. The NiO concentrations of the least depleted cpx-harzburgites are 0.15–0.43 wt.% and those of harzburgites and dunites are <0.27 wt.%, displaying a linear trend with the Mg# values (Fig. 3d). TiO_2 content is low in the cpx-harzburgites and most of the depleted harzburgites (<0.08 wt.%). However, some highly depleted harzburgite and dunite samples contain spinel with higher TiO_2 contents (up to 0.18 wt.%).

6. Whole-rock geochemistry

6.1. Whole-rock major and trace element geochemistry

Whole rock geochemical data of the selected samples are shown in Table 3, and a complete data set is given in Appendix 2. All samples analyzed have been serpentinized to varying extents (LOI = 0.90–16.59 wt.%). The low CaO contents (0.06–2.57 wt.%) are conformable with clinopyroxene abundance. The samples are Mg-rich (average MgO = 44.92 wt.%, $\sigma = 2.40$), Al-poor (average $Al_2O_3 = 0.79$ wt.%, $\sigma = 0.71$) and alkali-poor (average $Na_2O = 0.01$ wt.%, $\sigma = 0.02$).

Most of the peridotite samples from the Muğla ophiolite plot in the terrestrial mantle array (Hart and Zindler, 1986; Jagoutz et al., 1979) in the MgO/SiO_2 versus Al_2O_3/SiO_2 diagram (Fig. 5). However,

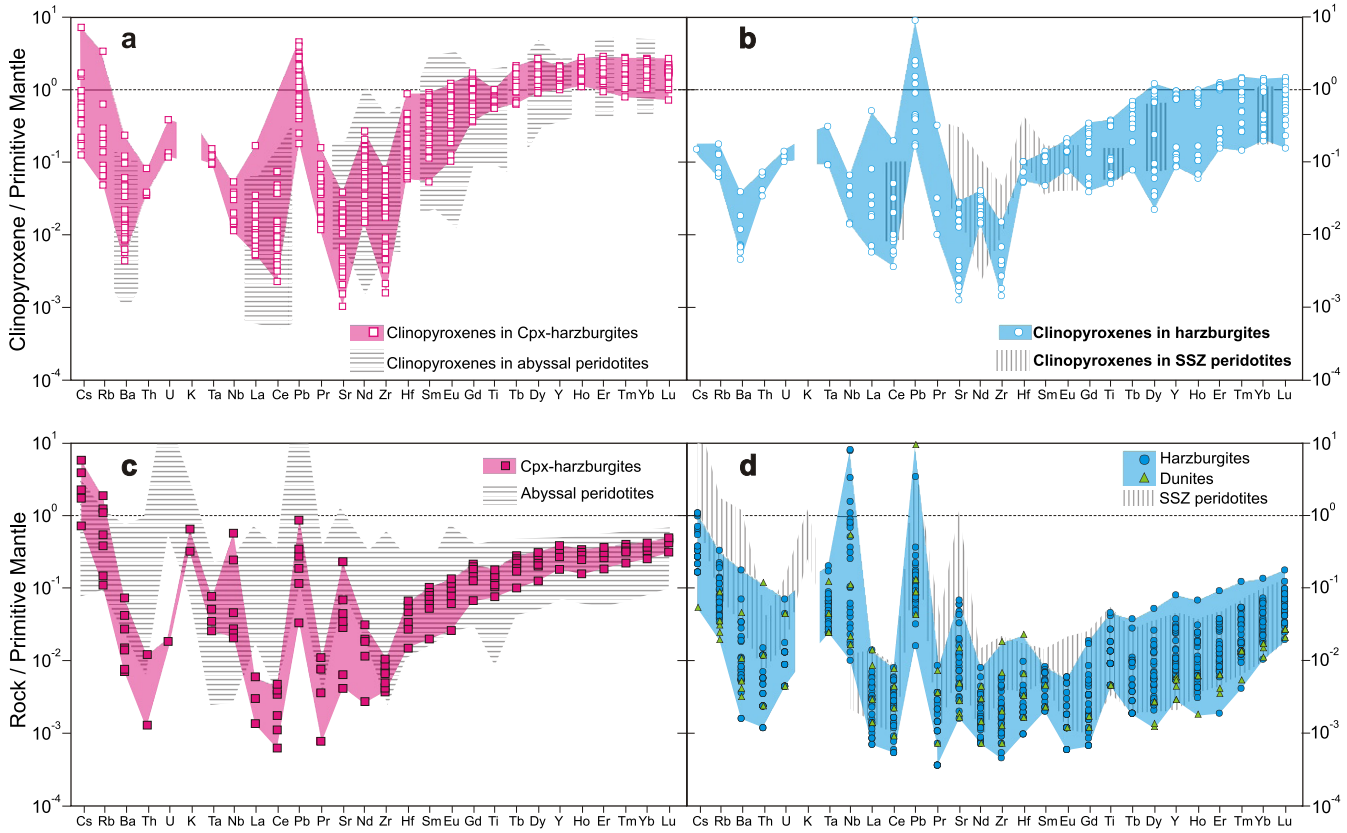

Fig. 4. Primitive mantle normalized multi-element spider diagrams for clinopyroxenes from the cpx-harzburgites (a) and depleted harzburgites (b), and whole-rock analyses from the cpx-harzburgites (c), depleted harzburgites and dunites (d).
Normalization factors are from Palme and O'Neill (2004). Abyssal peridotite fields are from Hellebrand et al. (2002), Johnson and Dick (1992) and Niu et al. (1997). SSZ (Izu–Bonin–Mariana Forearc) peridotite fields are from Parkinson and Pearce (1998).

Table 3
Whole rock major oxides (wt.%), trace elements and REE abundances (ppm) of representative peridotite samples from the Muğla. LOI: Loss on ignition; Mg# = (mol) 100MgO/(MgO + FeO); Serp% = (100/18) x LOI (wt.%); –: Below detection limit (see Appendix 2 for detection limits).

Sample	L18P	L42P	L48P	L5PB	L6PA	L15P	L38P	LYOL2	L16PB	L40P
Rock-type	Cpx-H	Cpx-H	Cpx-H	H	H	H	H	H	D	D
SiO_2	44.55	44.19	45.46	43.15	43.53	43.10	43.31	42.79	40.22	40.40
TiO_2	0.016	0.030	0.039	0.003	0.001	0.004	0.009	0.001	0.001	0.001
Al_2O_3	1.77	2.25	2.21	0.43	0.30	0.59	1.00	0.21	0.04	<0.01
Fe_2O_3	8.98	8.91	9.01	8.79	9.06	8.87	9.20	9.25	8.63	8.74
MnO	0.12	0.12	0.13	0.12	0.12	0.11	0.12	0.12	0.11	0.11
MgO	40.94	41.04	39.83	45.67	45.89	44.66	44.03	45.70	49.69	49.79
CaO	2.06	2.57	2.40	0.71	0.54	0.95	1.43	0.36	0.20	0.11
Na_2O	0.06	0.04	0.03	0.02	<0.01	<0.01	<0.01	<0.01	<0.01	<0.01
K_2O	0.02	<0.01	<0.01	<0.01	<0.01	<0.01	<0.01	<0.01	<0.01	<0.01
LOI	5.82	6.90	5.03	8.60	14.45	1.42	7.18	4.62	6.63	16.14
Σ	98.52	99.15	99.11	98.89	99.44	98.28	99.10	98.43	98.89	99.15
Mg#	89.0	89.1	88.7	90.3	90.0	90.0	89.5	89.8	91.1	91.0
Serp%	32.3	38.3	27.9	47.8	80.3	7.9	39.9	25.7	36.8	89.7
Sc	13.3	15.7	15.8	9.4	8.5	10.9	11.9	8.5	5.1	4.1
V	51.2	61.6	65.6	22.6	14.2	30.4	41.3	10.7	2.4	1.5
Cr	2631	3333	3079	2141	886	3006	3448	1095	442	250
Co	102.5	96.2	95.8	105.7	101.7	114.4	102.8	116.8	113.9	99.3
Ni	2739	2064	2122	2927	2888	3130	2207	3140	3729	2736
Cu	19.14	20.38	31.73	0.88	1.66	14.55	21.33	5.94	3.25	2.39
Zn	39.1	44.4	41.1	38.7	32.3	46.2	44.3	38.4	32.0	28.9
Ga	1.47	1.96	1.99	0.49	0.27	0.69	1.02	0.27	0.13	0.11
Rb	1.115	0.320	0.216	0.203	0.033	0.087	0.117	0.021	0.012	0.022
Sr	0.589	4.646	0.133	0.094	0.395	0.065	0.086	0.149	0.039	0.101
Y	0.796	1.618	1.492	0.065	0.024	0.113	0.360	0.024	0.013	0.024
Zr	0.041	0.069	0.074	0.011	0.010	0.023	0.029	0.015	0.008	0.076
Nb	0.145	0.016	0.028	0.011	–	0.304	–	–	–	0.010
Cs	0.103	0.013	–	0.018	0.003	0.012	0.004	0.003	–	–
Ba	0.486	0.049	0.095	0.142	0.036	0.074	0.044	0.040	0.036	0.022
La	0.0009	–	0.0040	0.0006	0.0007	0.0026	0.0010	0.0006	0.0010	0.0060
Ce	0.0011	0.0030	0.0060	0.0065	0.0048	0.0045	0.0030	0.0010	0.0017	0.0080
Pr	0.0002	0.0010	0.0010	0.0001	0.0001	0.0005	–	0.0001	0.0002	0.0010
Nd	0.0035	0.0260	0.0240	0.0018	0.0020	0.0031	0.0030	0.0012	0.0010	0.0040
Sm	0.0085	0.0340	0.0360	0.0022	0.0023	0.0019	0.0020	–	–	0.0010
Eu	0.0041	0.0180	0.0160	0.0002	0.0001	0.0004	0.0010	0.0001	0.0002	–
Gd	0.0375	0.1120	0.1000	0.0009	0.0006	0.0019	0.0110	0.0004	0.0007	–
Tb	0.0104	0.0260	0.0250	0.0004	0.0002	0.0009	0.0040	0.0003	–	–
Dy	0.0907	0.2070	0.1900	0.0052	0.0015	0.0091	0.0380	0.0018	0.0009	0.0020
Ho	0.0246	0.0500	0.0480	0.0019	0.0005	0.0031	0.0110	0.0007	0.0003	0.0010
Er	0.0858	0.1600	0.1510	0.0088	0.0036	0.0133	0.0430	0.0033	0.0017	0.0030
Tm	0.0158	0.0280	0.0260	0.0023	0.0009	0.0029	0.0090	0.0007	0.0004	0.0010
Yb	0.1144	0.1880	0.1740	0.0221	0.0106	0.0276	0.0640	0.0082	0.0053	0.0080
Lu	0.0220	0.0350	0.0330	0.0048	0.0030	0.0059	0.0130	0.0018	0.0015	0.0020
Hf	0.0045	0.0140	0.0170	0.0007	0.0003	0.0005	0.0010	0.0003	0.0005	0.0020
Ta	0.0014	0.0010	0.0020	0.0031	0.0021	0.0018	0.0010	0.0014	0.0018	0.0010
Pb	0.0625	–	0.0340	0.0524	0.0127	0.0310	0.0400	0.0144	1.7921	0.0080
Th	0.0001	–	0.0010	0.0001	0.0002	0.0004	–	0.0001	0.0002	0.0010
U	0.0004	–	–	0.0001	0.0001	0.0003	–	0.0003	0.0001	0.0010

some of the cpx-harzburgite and depleted harzburgite samples are represented by slightly lower MgO/SiO_2 values, which imply that these samples lost their Mg during sea floor alteration (Niu, 2004; Snow and Dick, 1995). Therefore, due to the influence of secondary events, some samples contain lower major and trace element concentrations than those estimated for a given degree of melting. In contrast, dunite samples have relatively higher MgO/SiO_2 values, which may suggest that the compositions of these samples are affected by the interaction of a later stage of olivine rich melt(s).

Taking into account that the peridotite samples are less affected by seafloor alteration, the most suitable method to examine the chemical changes of samples is to observe the variations of elements in each sample with respect to their Mg contents. Accordingly, MgO is used as an indicator of a degree of depletion and any increase in the MgO content reveals that the rock is more depleted, and therefore it is more enriched in olivine.

The TiO_2, Al_2O_3, Fe_2O_3 and CaO concentrations of the cpx-harzburgites are higher, whereas the NiO concentration is lower than those of the depleted harzburgites and dunites (Fig. 6). Although whole-rock Mg# values of the three different rock types are similar, the Mg# values of the cpx-harzburgites are in the range of 88.7–89.3, which tend, depending on the depletion extent, to increase towards the harzburgites (89.5–90.5) and dunites (90.4–92.8) (Appendix 2).

Except for Nb, Ta, La, and Ce, all other elements are correlated with the MgO content. Cobalt behaves in a compatible manner during partial melting and is positively correlated with MgO contents, while the elements incompatible for olivine and all REEs (except for La and Ce) are negatively correlated with the MgO contents (Fig. 7). The chalcophile elements, Cu and S, behave like Ca and Al during partial melting (e.g. Luguet et al., 2003); therefore, the Cu concentrations of the samples decrease with increasing degree of depletion, except in one harzburgite sample (L20P) that shows Cu enrichment (64.08 ppm). Figs. 6 and 7 also compare the Muğla peridotites with the abyssal (or Mid Ocean Ridge; MOR-type) and supra subduction zone (SSZ) type peridotites. Major and trace element abundances of the cpx-harzburgites, with higher MgO contents, closely resemble MOR-type peridotites, while depleted harzburgites and dunites are comparable to the SSZ-type peridotites.

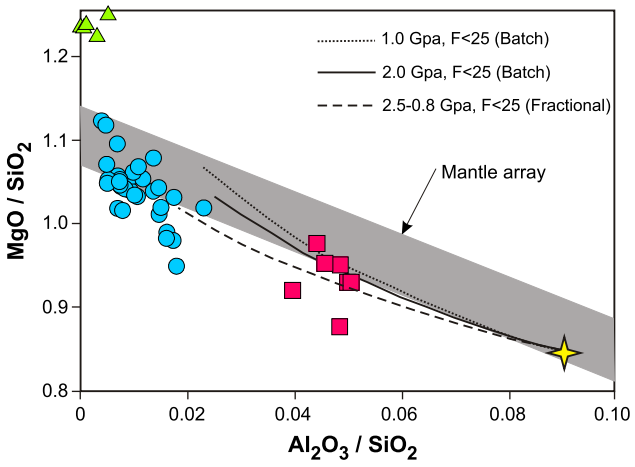

Fig. 5. MgO/SiO_2 vs. Al_2O_3/SiO_2 diagram for the Muğla peridotites. Mantle array is from Hart and Zindler (1986) and Jagoutz et al. (1979). Curves of polybaric near-fractional and isobaric batch melting of fertile mantle source (star) are from Marchesi et al. (2006) and Niu et al. (1997).

All peridotite samples are characterized by variously depleted REE patterns (Fig. 4c and d). The cpx-harzburgites display a continuous pattern of depletion from Lu to Ce that ends with a slight enrichment of La (Fig. 4c). The depleted harzburgite and dunite samples are characterized by (1) more depleted HREE contents and (2) sharper decrease from HREE to MREE with respect to those of the cpx-harzburgites (Fig. 4d). The depleted harzburgites and dunites are characterized by similar LREE concentrations, whereas MREE and HREE concentrations of the dunites are lower than those of the depleted harzburgites. In both rock types, LREE concentrations are generally increased compared to the MREE. The depleted harzburgites and dunites closely resemble the forearc peridotites with low REE contents, characterized by higher HREE concentrations (Fig. 4c and d).

The cpx-harzburgites are characterized by a slight negative Ti anomaly, whereas the depleted harzburgites and dunites show pronounced positive Ti anomalies. In addition, the cpx-harzburgites are characterized by clear depletion in Zr, whereas most of the depleted harzburgite and dunite samples display enriched or smooth patterns (Fig. 4d). All rock groups show pronounced peaks in Nb, Pb and Sr. The absence of a systematic relationship between LOI and Sr and Nb suggests that the observed anomalies are not caused by serpentinization.

6.2. Platinum group element (PGE) geochemistry

All rock samples of the Muğla peridotites have similar PGE abundances. Their total PGE contents are between 17 and 75 ppb, with an average concentration of 35 ppb (Table 4). All the cpx-harzburgite samples show negative Pt anomalies (0.49–0.71). Nevertheless, one sample (L42P) that was analyzed in both the Leoben University and the Genalysis Laboratories displays different Pt anomaly values ($Pt/Pt^* = 1.12$ and 0.49, respectively). This difference is attributed to the inhomogeneous distribution of base-metal minerals (BMM) by which Pt and Pd are

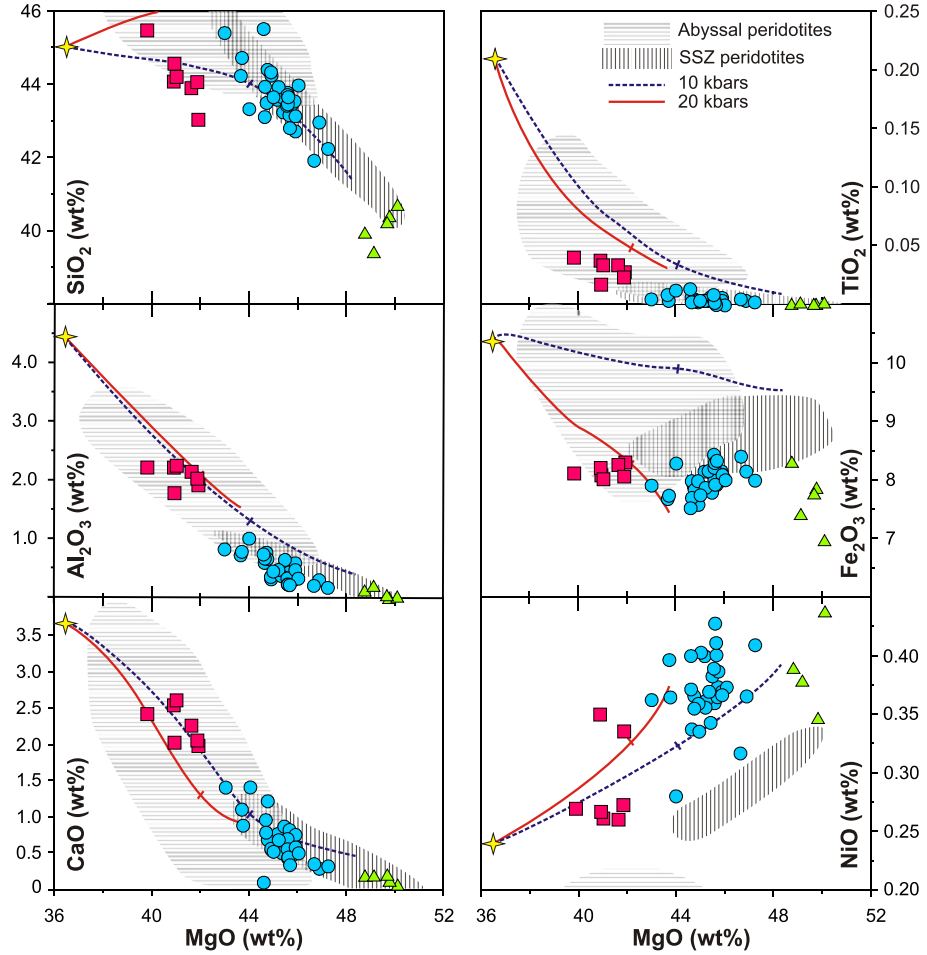

Fig. 6. Variation diagrams of MgO (wt.%) vs. selected major oxides in bulk rock peridotite samples of the Muğla ophiolite. Compositions are recalculated on a volatile free basis. Abyssal and SSZ peridotite fields are from Niu et al. (1997) and Parkinson and Pearce (1998), respectively. Also shown are residual compositions after from melting (at 10 and 20 Kb) of Primitive Mantle (Palme and O'Neill, 2004) calculated using pMELTS program for maximum 40% melting degree (Ghiorso et al., 2002). Clinopyroxene disappear after ~MgO = 44 for 10 Kb and ~MgO = 42 for 20 Kb (indicated by ticks on melting curves).

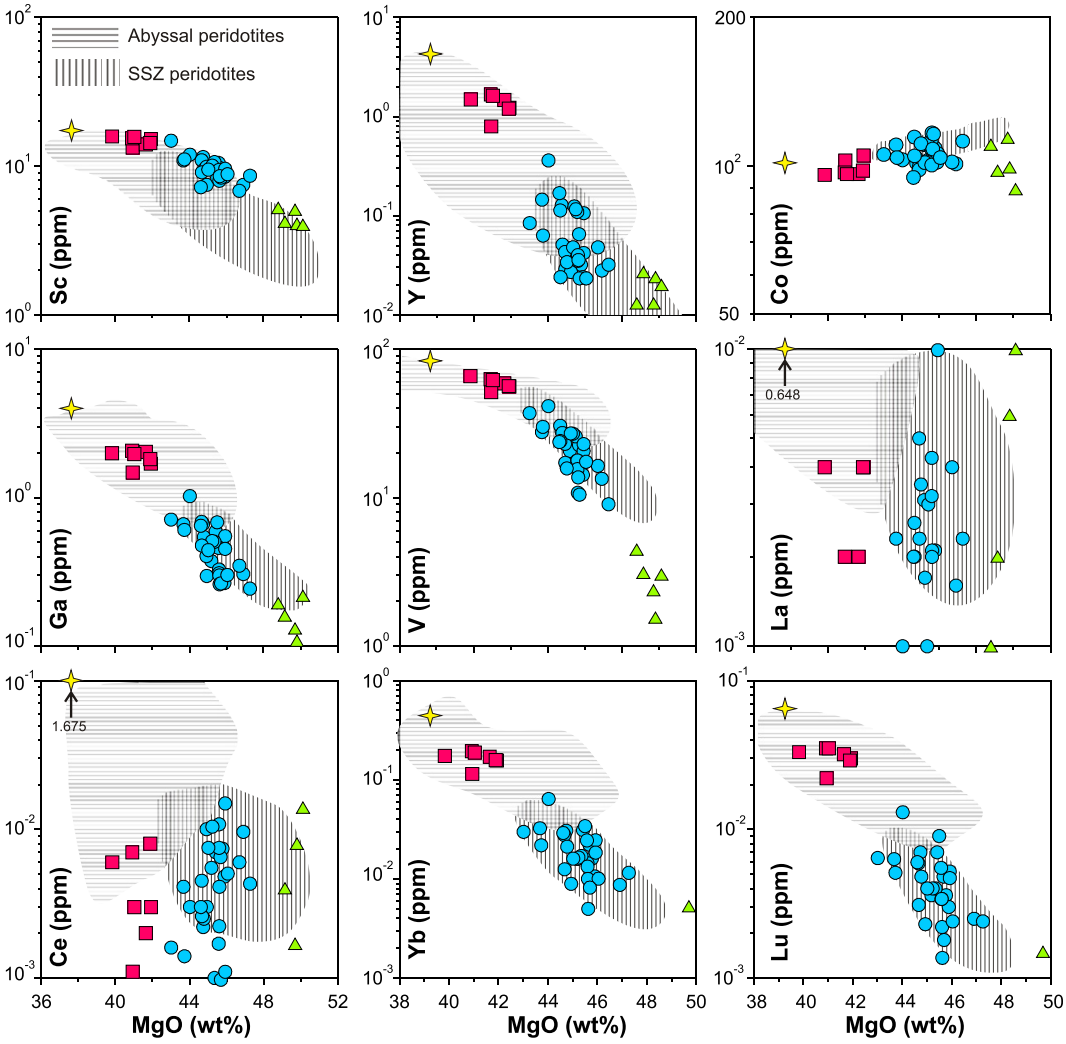

Fig. 7. Variation diagrams of MgO vs. selected trace and rare earth elements in bulk rock peridotite samples of the Muğla ophiolite. Abyssal and SSZ peridotite fields are from Niu et al. (1997) and Parkinson and Pearce (1998), respectively.

transported (Lorand et al., 2008; Meisel et al., 2003). Slightly positive Pt anomalies were observed in 4 out of the 17 depleted harzburgite samples ($Pt/Pt^* = 1.19–1.41$). All the other depleted harzburgite and dunite samples display negative Pt anomalies ($Pt/Pt^* = 0.49–0.92$). The Pd/Ir values of cpx-harzburgites are between 1.55 and 4.00 (Table 4). In mantle-normalized PGE diagrams, these data yield a slight positive trend from Os to Pd (Fig. 8). The Pd/Ir ratios of the depleted harzburgites and dunites are 0.35–6.40, a wider range when compared to the cpx-harzburgites. Therefore, in chondrite-normalized PGE plots the depleted harzburgites and dunites are characterized by a positive trend from Os to Rh and a negative trend from Rh to Pt, whereas some samples are also represented by positive to negative anomalies from Pt to Pd.

Comparison of chondrite-normalized PGE plots of the Muğla peridotites with those from the Uralian–Alaskan type ultramafic rocks, which are characterized by positive Pt anomalies, reveals no similar trends. However, almost all the peridotites we have analyzed are similar to the harzburgites and dunites of the subduction-related, Mesozoic Vourinos (Greece), Troodos and Mamonia (Cyprus) ophiolites (Fig. 8). One of the harzburgite samples displays a positive trend with a Pd/Ir ratio of 6.40, and also has the highest Cu concentration of 64 ppm. This Cu enrichment might be explained by the presence of Cu-rich sulfides since these sulfides are the potential host for Pd (Ballhaus et al., 2006; Bockrath et al., 2004; Lorand and Alard, 2001).

PGE abundances of selected Muğla samples are plotted against their Al_2O_3 (wt.%) contents, on which partial melting trends of primitive mantle (PM) source are also shown (Fig. 9). PGE concentrations of the dunites and harzburgites with lower Al_2O_3 contents are characterized by nearly the same or higher concentrations when compared with the cpx-harzburgites. Therefore, there is a negative correlation between the PGE and Al_2O_3 contents of the Muğla peridotites.

6.3. Re–Os isotope systematics

We analyzed ten selected peridotite samples for their Re, Os and Os-isotopic compositions (Table 4). The concentrations of Os and Re are 4.0–6.6 and 0.05–1.95 ppb, respectively. Fig. 10a shows that there is a negative correlation between Re and Al_2O_3 concentrations; however, some samples have higher Re concentrations scattering above the depletion line, which is plotted according to non-modal dynamic melting of PM (melting parameters are from Batanova et al., 2008). The $^{187}Os/^{188}Os$ ratios of the depleted harzburgite samples and one cpx-harzburgite (0.10792–0.12746) are lower than the present day chondritic values (0.1275; Walker et al., 1989) and the PM (0.1296; Meisel et al., 2001). However, the $^{187}Os/^{188}Os$ ratios of two cpx-harzburgite samples (0.12910 and 0.12952) are determined to be higher than the present day chondritic value but very close to the PM value. The initial Os-isotopic compositions of the cpx-harzburgites are 0.12497–0.12858 ($\gamma Os = -0.79$ to $+2.08$) for an age of 250 Ma, which corresponds in general to the timing of the

Table 4
PGE and Re concentrations (ppb), and Re–Os isotopic data of the selected peridotite samples from the Muğla ophiolite.

Sample	Rock-type	Cr#	Os	Ir	Ru	Rh	Pt	Pd	Re	Re[a]	PGE	Pd/Ir	ΣPGE	Pt/Pt*	Re/Os	$^{187}Os/^{188}Os$	$^{187}Re/^{188}Os$	$^{187}Os/^{188}Os_i$ (at 250 Ma)	γOs	T_{RD}	T_{MA}[b]
JP-1[c]	Standard		3.25	3.28	4.92	1.09	4.96	1.20	0.06							0.12260					
RSD%	Standard		0.4	0.4	0.7	0.01	0.4	0.7	0.6							1.2					
L18P	Cpx-H	20.9	4.0	4.0	12.0	2.0	11.0	10.0			43	2.50	43	0.65							
L32P	Cpx-H	17.9	<2.0	3.0	8.0	2.0	9.0	8.0			30	2.67	30	0.60							
L35P[c]	Cpx-H	16.2	4.0	3.2	5.9	1.2	6.1	6.2	0.36	0.20	27	1.92	27	0.59	0.091	0.12910	0.434	0.12809	1.69	*f*	*f*
L42P[c]	Cpx-H	15.2	4.3	4.1	7.7	1.4	13.5	7.3	0.41	0.20	38	1.79	38	1.12	0.095	0.12952	0.460	0.12858	2.08	*f*	*f*
L42P	Cpx-H	15.2	<2.0	3.0	8.0	2.0	9.0	12.0			34	4.00	34	0.49							
L47P[c]	Cpx-H	18.6	5.0	4.3	7.9	1.3	7.9	6.7	1.07	0.11	33	1.55	33	0.71	0.216	0.12573	1.031	0.12497	−0.79	274	376
L48P	Cpx-H	17.5	<2.0	4.0	9.0	2.0	9.0	10.0			34	2.50	34	0.53							
L1PA[c]	Hzb	58.8	6.6	5.1	9.4	3.1	10.4	6.9	0.30	0	41	1.36	41	0.60	0.045	0.12078	0.219	0.12078	−4.11	1014	1014
L1PA	Hzb	58.8	4.0	5.0	12.0	3.0	13.0	11.0			48	2.20	48	0.60							
L5PA[c]	Hzb	64.0	6.1	3.9	8.3	1.5	6.2	2.7	1.95	0	29	0.69	29	0.82	0.320	0.10792	1.537	0.10792	−14.32	2892	2892
L30P[c]	Hzb	56.6	2.3	2.6	4.1	1.3	5.6	0.9			17	0.35	17	1.35							
L5PB[c]	Hzb	54.7	5.1	3.5	6.5	1.5	8.6	2.5	0.06	0	28	0.70	28	1.19	0.012	0.12270	0.057	0.12270	−2.59	728	728
L6PB[c]	Hzb	52.2	5.5	4.2	7.3	1.3	7.9	5.1	0.14	0	31	1.23	31	0.80	0.026	0.12163	0.123	0.12145	−3.45	747	750
L14P[c]	Hzb	46.1	5.2	3.9	7.7	1.4	7.9	8.1	0.17	0.01	34	2.10	34	0.61	0.033	0.12746	0.158	0.12719	−0.98	14	14
L28P[c]	Hzb		4.9	3.2	7.9	1.4	7.9	1.6	0.05	0	27	0.49	27	1.41	0.011	0.12479	0.049	0.12479	−0.93	416	416
L10P	Hzb	53.1	4.0	5.0	11.0	3.0	12.0	12.0			47	2.40	47	0.53							
L11P	Hzb	59.3	<2.0	5.0	11.0	2.0	11.0	12.0			41	2.40	41	0.59							
L16PA	Hzb	52.7	<2.0	4.0	11.0	2.0	11.0	3.0			31	0.75	31	1.19							
L38P	Hzb	37.6	4.0	4.0	9.0	2.0	9.0	10.0			38	2.50	38	0.53							
LYOL3	Hzb	58.3	4.0	4.0	10.0	1.0	6.0	3.0			28	0.75	28	0.92							
L3P[c]	Hzb	66.4	5.0	3.6	6.2	1.0	4.5	1.7	0.05	0	22	0.48	22	0.89	0.010	0.12588	0.048	0.12588	−0.06	252	252
L20P	Hzb	73.4	6.0	5.0	11.0	3.0	18.0	32.0			75	6.40	75	0.49							
LYOL2	Hzb	76.2	9.0	6.0	20.0	1.0	<2.0	3.0			39	0.50	39								
L16PB	Dun	74.8	4.0	5.0	6.0	2.0	5.0	3.0			25	0.60	25	0.54							

γOs is calculated using the parameters from Shirey and Walker (1998) and λ for $^{187}Re = 1.666 \times 10^{-11}$ a^{-1} (Smoliar et al., 1996). JP-1: peridotite standard collected at Horoman in the Hokkaido Island in Japan. *f*: future age. $Pt/Pt^* = (Pt/8.3)/[(Rh/1.6) \times (Pd/4.4)]^{1/2}$.

[a] Re concentrations are corrected by extraplotting the Re concentrations to melting curve on Re vs. Al_2O_3 diagram (see Fig. 10), following Batanova et al. (2008).

[b] Modal ages are calculated using corrected Re concentrations.

[c] PGE and Os isotope data were measured at Leoben University, Leoben, Austria.

opening of the Neo-Tethys in the broader eastern Mediterranean region (Lapierre et al., 2004 and references therein). These values correspond to an Os-isotopic composition of a chondritic source that is computed for 250 Ma (Shirey and Walker, 1998). However, the $^{187}Os/^{188}Os_{(i)}$ ratios of the depleted harzburgites are slightly lower and are in the range of 0.12078–0.12719 (γOs = −4.11 to −0.06). Sample L5PA has very low $^{187}Os/^{188}Os_{(i)}$ value of 0.10792 (γOs = −14.32), which also has very high Re (1.95 ppb) and has been excluded in related figures (see Discussion). In comparison to the depleted harzburgites, the cpx-harzburgites tend to have higher $^{187}Os/^{188}Os_{(i)}$ (for 250 Ma) ratios, and hence there is a negative correlation between the Cr# values of spinels and the $^{187}Os/^{188}Os_{(i)}$ ratios (Fig. 10b). The poor correlation between $^{187}Os/^{188}Os$ and $^{187}Re/^{188}Os$ shows that the Re contents were disturbed by later events. This phenomenon prevents dating of the analyzed rocks by the Os-isotopic data (Fig. 10c). The $^{187}Re/^{188}Os$ ratios of the cpx-harzburgites (0.434–1.031) are greater than those of the depleted harzburgites (0.0486–0.219) and PM (~0.40; Meisel et al., 2001).

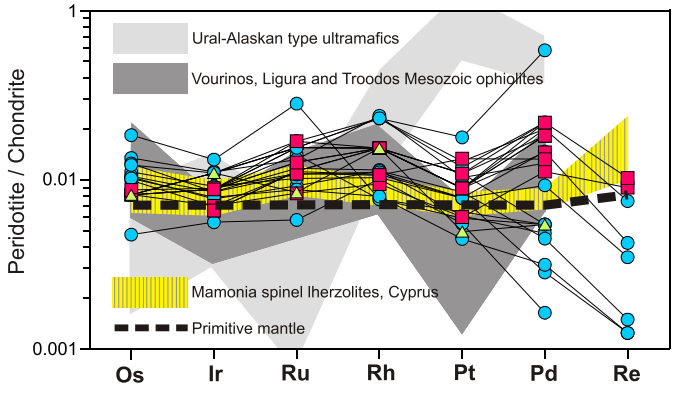

Fig. 8. Chondrite-normalized PGE abundances of mantle peridotites from the Muğla ophiolite. Thick dotted line shows the composition of primitive mantle after (McDonough and Sun, 1995). Yellow area shows compositions of Mamonia spinel lherzolites (Batanova et al., 2008). Also plotted for comparison are Ural–Alaskan type ultramafic rocks (light gray field) and Mesozoic ophiolites of Vourinos, Ligura and Troodos (dark gray field). Fields are taken from Garuti et al. (1997). (For interpretation of the references to color in this figure legend, the reader is referred to the web version of this article.)

7. Discussion

7.1. Partial melting processes and geodynamics

The clinopyroxene content of peridotites reflects only the degree of depletion. Since the equilibrium between olivine and melt remains unchanged by H_2O input (Gaetani and Grove, 1998), the forsterite composition of olivine yields the total degree of partial melting. Based on these criteria, we determine that the Muğla peridotites containing varying amounts of clinopyroxene (up to 5 vol.%) and olivine with high forsterite compositions (90.8–92.6) were subjected to different degrees of partial melting. It is known that Al contents of pyroxene and spinel are sensitive to the partial melting of mantle rocks and that they are systematically decreased as the peridotites become more depleted (e.g. Dick and Natland, 1996; Zhou et al., 2005). The Al_2O_3 contents of clinopyroxene within the Muğla peridotites are negatively correlated with the Cr# values of spinel with which they were equilibrated. The clinopyroxene in the cpx-harzburgites is represented by high Al_2O_3 contents, and the spinel grains in equilibrium with these minerals have low Cr# values (Fig. 11a). The Al_2O_3 vs. TiO_2 contents of clinopyroxenes of all the rocks ranging from the cpx-harzburgites to the depleted harzburgites and dunites show variations consistent with an increase in the degree of partial melting of peridotitic rocks (Fig. 11b). The Cr# and Mg# values of spinels are negatively correlated (not shown), suggesting that these rocks were produced by different degrees of partial melting. Okamura et al. (2006) explain the low Mg# of spinel from the

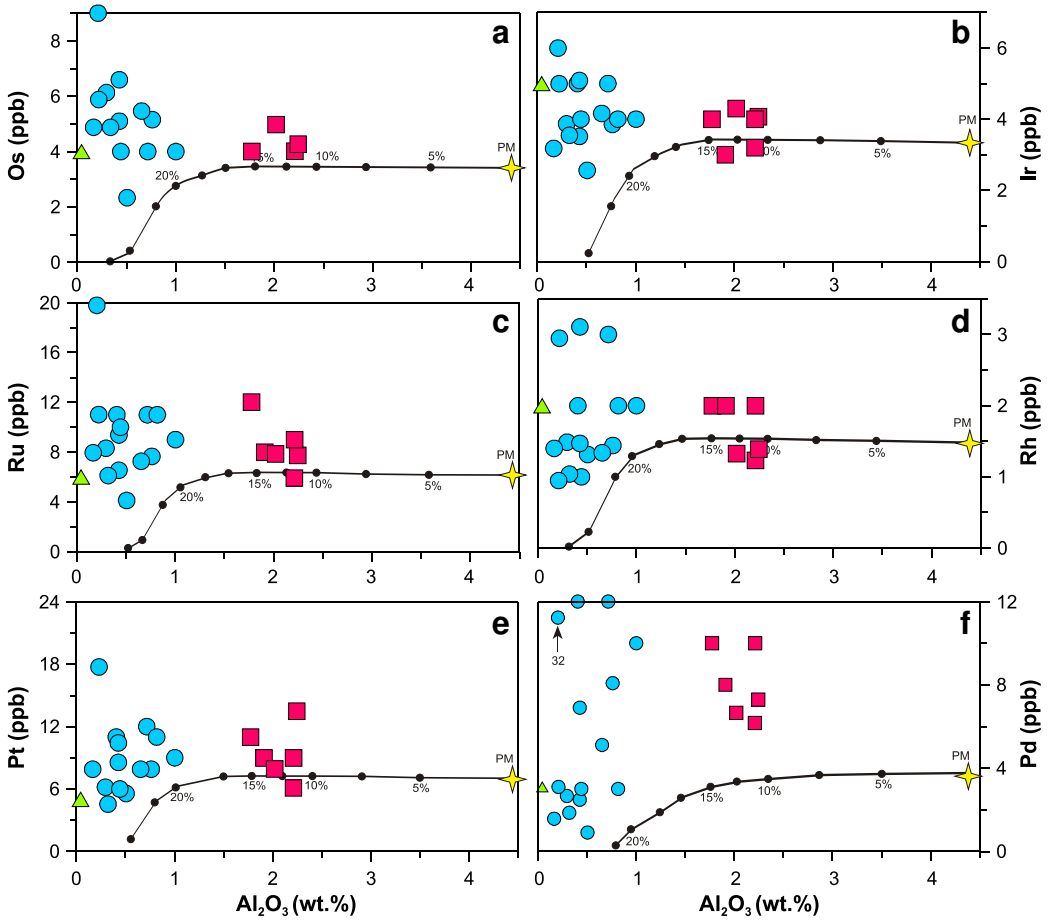

Fig. 9. Variation of Os, Ir, Ru, Rh, Pt, and Pd against Al_2O_3 (wt.%) in peridotite samples of the Muğla ophiolite. Primitive mantle compositions (yellow star) are from McDonough and Sun (1995), and curves representing modeled variations of PGEs within a mantle residue experienced progressive melt extraction are taken from Aldanmaz and Köprübaşı (2006). Dots on melt extraction curves indicate melting increments in percent. (For interpretation of the references to color in this figure legend, the reader is referred to the web version of this article.)

depleted harzburgite and dunite rocks from the Hahajima Seamount Izu–Bonin arc as a result of cooling of the mantle wedge peridotites beneath a forearc setting by H_2O released from the subducted slab. The correlation between the Cr# values of spinels and the forsterite composition of olivines reveals that the trend of samples under investigation is conformable with the olivine–spinel mantle array (OSMA; Arai, 1994). This trend confirms that the Muğla peridotites are the residues of various degrees of melt extraction (Fig. 11c). We conclude, therefore, that the cpx-harzburgites of the Muğla peridotites are the residues of low-degrees partial melting, whereas the depleted harzburgites and dunites are the residues of higher degrees of partial melting.

7.2. Oxygen fugacity

In order to calculate the oxygen fugacity, we measured the olivine–orthopyroxene–spinel associations. We used the formulas of Ballhaus et al. (1991) and Nell and Wood (1991) that are based on the reaction of $6Fe_2SiO_4 + O_2 = 3Fe_2Si_2O_6 + 2Fe_3O_4$. Oxygen fugacity values calculated on the basis of average mineral composition are given in Table 5 as deviations ($\Delta \log fO_2^{FMQ}$) from the FMQ (fayalite–magnetite–quartz) buffer.

It is widely accepted that mantle wedge peridotites above subduction zones are more oxidized than upper mantle peridotites in other tectonic settings (e.g. Parkinson and Arculus, 1999). Moreover, H_2O derived from the dehydration of subducting oceanic lithosphere plays an important role in the formation of subduction-related melts and is thought to be an important oxidizer in the transformation of ferrous iron to ferric iron in subduction zones (Arculus, 1994). Calculated oxygen fugacities for the depleted harzburgites and dunites (−2.05 to +1.42) from the Muğla peridotites are positively correlated with Cr# of spinel (Fig. 12a). This relationship supports the notion that these melts, together with subduction-related magmas and fluids, interacted with the upper mantle rocks in the wedge during their rise to the surface. However, the cpx-harzburgites are also represented by a wide range of oxygen fugacities (−1.60 and +1.44) but a low and almost constant Cr# of spinel composition, which was attributed to fluid–solid interaction (Aldanmaz et al., 2009).

On the V–MgO diagram proposed by Lee et al. (2003), most of the cpx-harzburgites and some of the depleted harzburgites plot between the FMQ and FMQ-1 trends (Fig. 12b). However, two of the cpx-harzburgite samples, most of the depleted harzburgites and all dunite samples are plotted between the FMQ and FMQ+1 trends. These data are not within the oceanic mantle array shown in the same figure and reflect lower V contents. Since Fe^{3+} activity is mostly a sign of metasomatic processes, the fO_2 value, which is determined thermodynamically in the subduction zone peridotites, could be significantly higher than the fO_2 value obtained using the V content, which reflects oxygen fugacity records during partial melting (Lee et al., 2003). However, in the present study, oxygen fugacity estimations performed on the basis of mineral compositions and V systematics are found to be consistent with each other (Fig. 12a and b).

In light of the data and discussion summarized above, we conclude that the cpx-harzburgites in the Muğla peridotites are the products of low-degrees of partial melting (first-stage melt extraction), and are

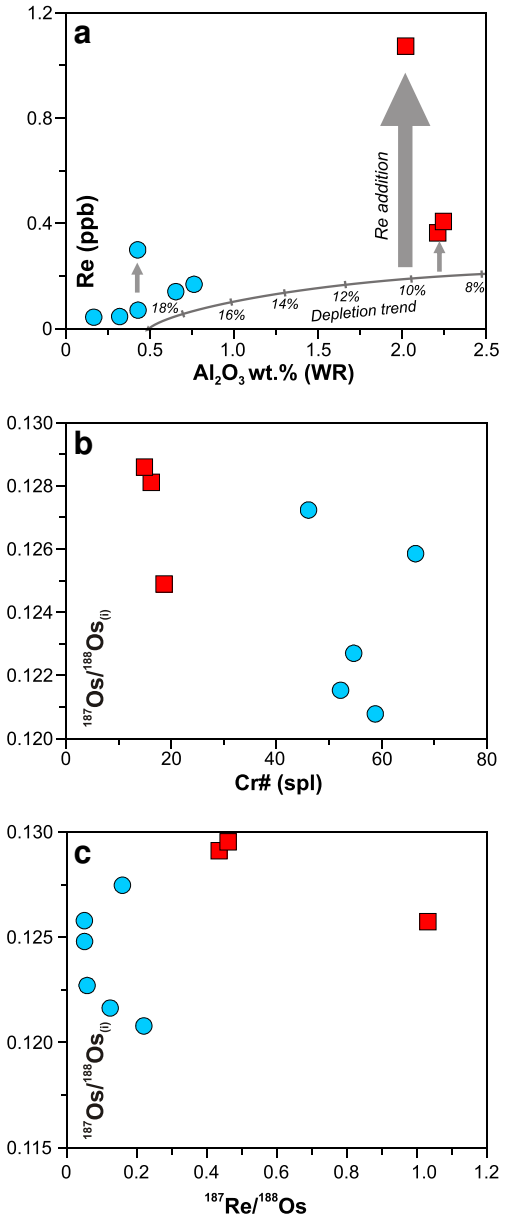

Fig. 10. Covariations of whole rock Al_2O_3 (wt.%) vs. Re (ppb) (a), Cr# of spinel vs. whole rock $^{187}Os/^{188}Os_{(i)}$ (b), and $^{187}Re/^{188}Os$ vs. $^{187}Os/^{188}Os$ (c) in selected peridotite samples. Depletion trend on (a) is plotted according dynamic melting of PM (with 1% porosity) by using partition coefficients of Adam and Green (2006) and Batanova et al. (2008).

most likely to have formed in a MOR environment. In contrast, the depleted harzburgites and dunites are more likely derived from remelting (second-stage melt extraction) of the cpx-harzburgites in a SSZ environment, producing boninite-like melts.

7.3. Melt–peridotite interaction and metasomatic signature

Very high Cr# values (~83) and low TiO_2 (<0.08 wt.%) contents of spinels in most of our depleted harzburgites may indicate that (1) they are residuals from high-degrees of partial melting, or (2) they are associated with boninitic melts. Mantle peridotites containing spinels with Cr#>70 are expected to have been derived from high degrees of partial melting yielding pyroxene-free dunites. However, some of the Muğla peridotites having spinels with very high Cr# (>70) are found to be harzburgite in character (Fig. 11c and d). This would appear to be inconsistent with a simple partial melting history in their genesis and may be attributed to refertilization processes (Barth et al., 2003; Godard et al., 2008). The presence of interstitial clinopyroxene and symplectitic clinopyroxene and spinel in some samples, and the presence of high TiO_2 spinels (up to 0.18 wt.%) in them support the above discussion (Fig. 2c, g and h).

Chromitite masses in the Muğla peridotites are high-Cr (Cr#>60) in composition and are surrounded by a dunitic envelope (Uysal et al., 2009). The clinopyroxene abundances in the peridotites increase away from these chromitite masses. Assuming that the cpx-harzburgites are the remnants of the first-stage of partial melting and the high-Cr chromitites are derived from a boninitic melt formed during the second-stage of partial melting of a previously depleted mantle (Uysal et al., 2009), the dunite envelope around the chromitites is likely to have resulted from incongruent melting of pyroxene as a result of interaction between the mantle peridotites and the boninitic melt (Dilek and Morishita, 2009). This incongruent melting may have produced olivine and SiO_2-rich melt, which is important for the formation of chromitites.

Spinel grains found in the cpx-harzburgites and most of the depleted harzburgites have a wide range of Cr# values (13–77) and are represented by low-Ti contents (<0.08 wt.% TiO_2). On the other hand, spinels in chromitites that crystallized from melts by second-stage partial melting have a narrow range of Cr# values (64–86) and high-Ti contents (<0.28 wt.% TiO_2) (Fig. 11c). Some of the highly depleted harzburgite and dunite samples appear to be impregnated by boninitic melts, from which the Muğla chromitites precipitated. The TiO_2 contents of the spinels in these samples increase towards the compositions of the Muğla chromitites. This trend is well explained by a reaction that took place between the old MOR-type peridotites (cpx-harzburgites) and the boninitic melt (Fig. 11c). In this case, Al-rich spinels in the peridotites were modified by the boninitic melt from which high-Cr chromitites were crystallized. During the course of this melt–peridotite interaction, the Cr/Al ratio of spinels was increased towards the chromitite mass. As a result, except for the clinopyroxene-rich samples, all other analyzed rocks that interacted with boninitic melts and fluids were depleted to varying extents. This interpretation is also supported by positive correlation between the oxygen fugacity and Cr# of spinels (Fig. 12a) of the depleted harzburgite and dunite samples, implying that the composition of spinel was affected by the melt–wall rock interaction (c.f., Pearce et al., 2000).

Enrichment in most of the incompatible elements in some of the cpx-harzburgites may be interpreted as a result of this melt–wall rock interaction after the first-stage melting (Fig. 4c). These incompatible elements could easily be enriched by low-degree partial melts derived from a deeper mantle and could subsequently react with the overlying depleted mantle (see next section).

The depleted harzburgites and dunites, resembling subduction zone peridotites, are represented by a clear depletion of MREE with respect to HREE (Fig. 4d). In addition, significant enrichments of LILE, LREE and some HFSE are consistent with a possible interaction of these peridotites with fluids or melts derived from the subducted slab (e.g. Kelemen et al., 1992; Parkinson and Pearce, 1998). Some boninitic rocks recovered from the Izu–Bonin–Mariana forearc setting were found to be enriched in Zr, Sr and LREE (Parkinson and Pearce, 1998). Partial enrichment of LREE and incompatible elements (Rb, Ba, Th, Nb and Sr; Fig. 4d) is believed to result from the interaction of boninitic magmas with peridotites in a mantle wedge.

7.4. Trace element constraints

In order to constrain the mode and nature of petrological processes during the genesis of the Muğla peridotites, we have performed several melting and enrichment models including closed- and open-system dynamic melting and melt percolation, using whole rock and clinopyroxene trace element contents (Fig. 13 and Appendix 3). The cpx-

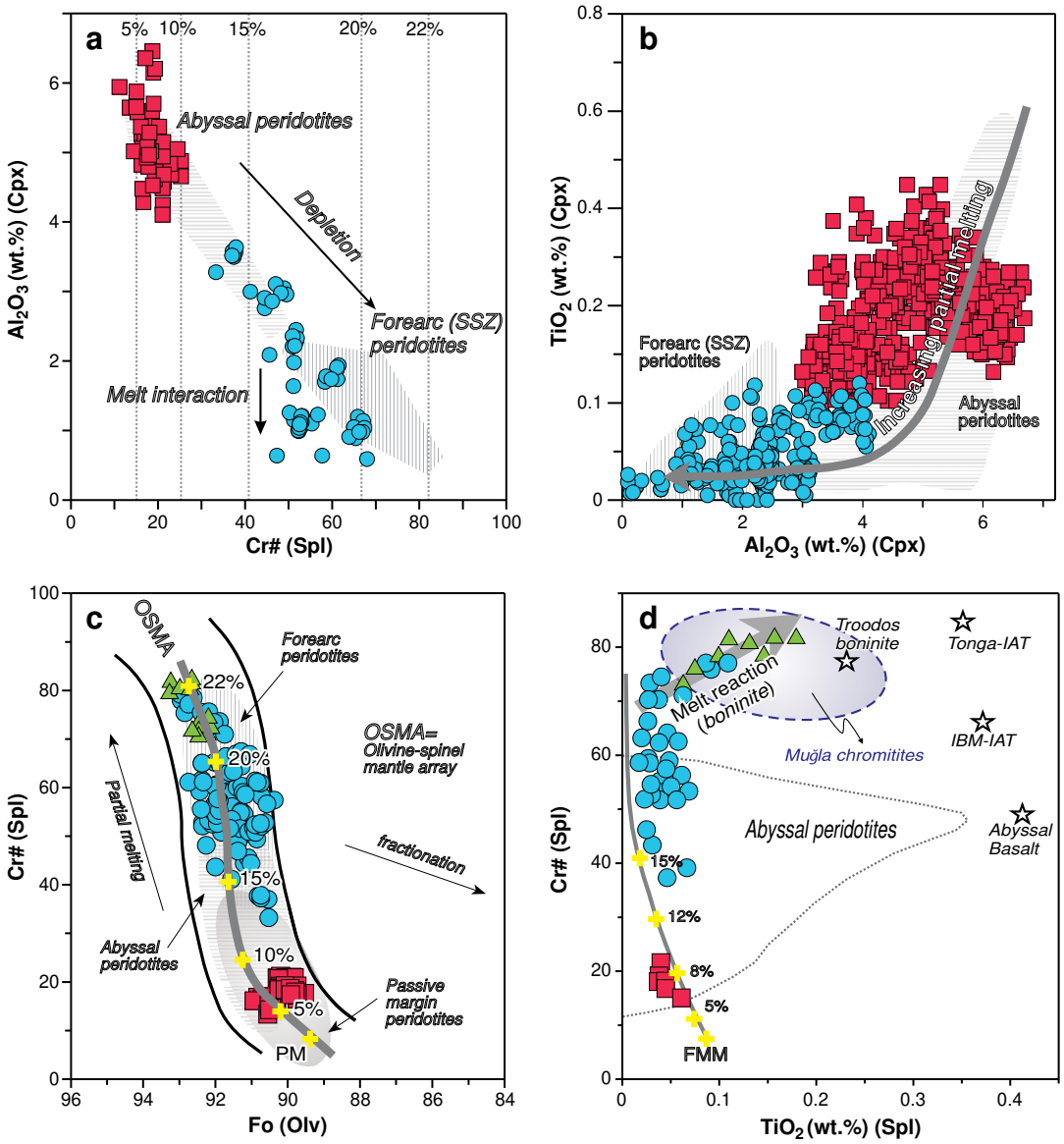

Fig. 11. (a) Bivariation diagram of Al_2O_3 (wt.%) of clinopyroxene vs. Cr# [100Cr/(Cr + Al)] of coexisting spinel for the Muğla peridotites. (b) TiO_2 (wt.%) vs. Al_2O_3 (wt.%) contents in clinopyroxene of peridotite samples. (c) Compositional relationship between Cr# of spinel and Fo [100 Mg/(Mg + Fe^{2+})] content of coexisting olivine (Arai (1992)) in peridotite samples. PM: Primitive Mantle. (d) Compositional variations of Cr# vs. TiO2 (wt.%) content of spinels (Pearce et al., 2000) in peridotite samples of the Muğla ophiolite.
Fields for passive margin, abyssal and forearc peridotites are taken from Dick and Bullen (1984), Bonatti and Michael (1989), Hebert et al. (1990), Johnson et al. (1990), Ishii et al. (1992), Arai (1994), Parkinson and Pearce (1998), Pearce et al. (2000) and Parkinson et al. (2003). Muğla chromitite field is after Uysal et al. (2009). The degrees of melt extractions are calculated on the basis of spinel composition using the empirical formula of Hellebrand et al. (2001).

harzburgite samples from the Muğla peridotites are less depleted with respect to the harzburgites and dunites that we analyzed. The whole rock and mineral chemistry of the cpx-harzburgites indicates that they are most probably abyssal-type peridotites, which underwent depletion in a mid ocean ridge system. Therefore, we first applied a closed-system dynamic melting model of a PM source (Palme and O'Neill, 2004) on a Ni/Yb vs. Yb diagram, as these elements are less sensitive to melt–rock interaction or mantle metasomatism and are useful to monitor the degree of partial melting (Fig. 13a). The results show that the cpx-harzburgites are the residuals of ~10–16% partial melting of PM. This range of partial melting is also applied on a PM-normalized REE diagram. Except for the LREE especially La, the REE abundances of the cpx-harzburgites are well-produced (Fig. 13b). Such a difference may be a consequence of melt–rock interactions in an oceanic environment; therefore, we also have modeled a melt–rock interaction on Fig. 13b. In this model, low degree (0.1%) partial melts from the deeper fertile mantle (PM) interact with the overlying depleted mantle (16% depleted PM is used) with a mixing ratios of 0.02% (model A) and 0.002% (model B). Model B on Fig. 13b explain well the lower bound of the REE abundances of the cpx-harzburgites, and the processes for the Model B are attributed to a first-stage melting and enrichment event in the genesis of the Muğla peridotites.

The harzburgites and dunites of the Muğla peridotites are analogous to SSZ-type peridotites on the basis of their whole rock and mineral chemistry, and are more depleted with respect to the cpx-harzburgites. Therefore, assuming that the harzburgites and dunites are the residuals of partial melting of the cpx-harzburgites that occurred in a SSZ environment, closed-system dynamic melting of Model B (obtained from 15% depletion of PM) can be applied (Fig. 13c). The Ni/Yb vs. Yb systematics of the harzburgites and dunites are well produced indicating that they are the ~10–24% partial melting residuals of the cpx-harzburgites. Around 10–16% closed-system dynamic melting of the Model B can explain the HREE concentrations of the harzburgites and dunites, but fails to replicate their LREE abundances (Fig. 13d).

Table 5
Calculated oxygen fugacities ($\Delta \log fO_2^{FMQ}$) for the Muğla peridotite samples (NW'91: Nell and Wood, 1991; Ba'91: Ballhaus et al., 1991).

Sample	Rock type	Spinel *Cr#*	Spinel $Fe^{3+}/\Sigma Fe$	Olivine *Fo*	Opx $X_{Fe}^{M1}X_{Fe}^{M2}$	NW'91 fO_2 $\Delta \log$ ^{FMQ}	Ba'91 fO_2 $\Delta \log$ ^{FMQ}
L18P	Cpx-harzburgite	21	0.174	90.0	0.0093	0.78	0.22
L32P	Cpx-harzburgite	18	0.088	90.1	0.0086	−0.46	−1.03
L35P	Cpx-harzburgite	16	0.119	90.6	0.0077	−0.06	−0.68
L42P	Cpx-harzburgite	15	0.104	90.5	0.0079	−0.05	−0.69
L47P	Cpx-harzburgite	19	0.150	90.0	0.0083	0.42	−0.01
L48P	Cpx-harzburgite	18	0.095	89.8	0.0090	−0.55	−1.09
L1PA	Harzburgite	59	0.110	91.6	0.0068	0.13	−0.40
L5PA	Harzburgite	64	0.107	91.8	0.0064	0.24	−0.33
L5PB	Harzburgite	55	0.097	91.4	0.0071	0.13	−0.26
L6PB	Harzburgite	52	0.054	91.5	0.0063	−1.28	−1.72
L10P	Harzburgite	53	0.113	91.3	0.0066	−0.22	−0.65
L11P	Harzburgite	59	0.094	91.2	0.0067	−0.38	−0.75
L14P	Harzburgite	46	0.138	91.2	0.0069	0.30	−0.09
L15P	Harzburgite	51	0.116	91.4	0.0071	0.22	−0.26
L16PA	Harzburgite	53	0.036	90.8	0.0072	−2.27	−2.69
L30P	Harzburgite	57	0.099	92.0	0.0066	0.17	−0.47
L38P	Harzburgite	38	0.050	90.8	0.0081	−1.49	−2.08
LYOL3	Harzburgite	58	0.091	92.4	0.0063	0.12	−0.65
L3P	Harzburgite	66	0.083	91.5	0.0066	−0.31	−0.83
L20P	Harzburgite	73	0.116	92.0	0.0048	0.37	0.18
LYOL2	Harzburgite	76	0.115	92.6			0.07

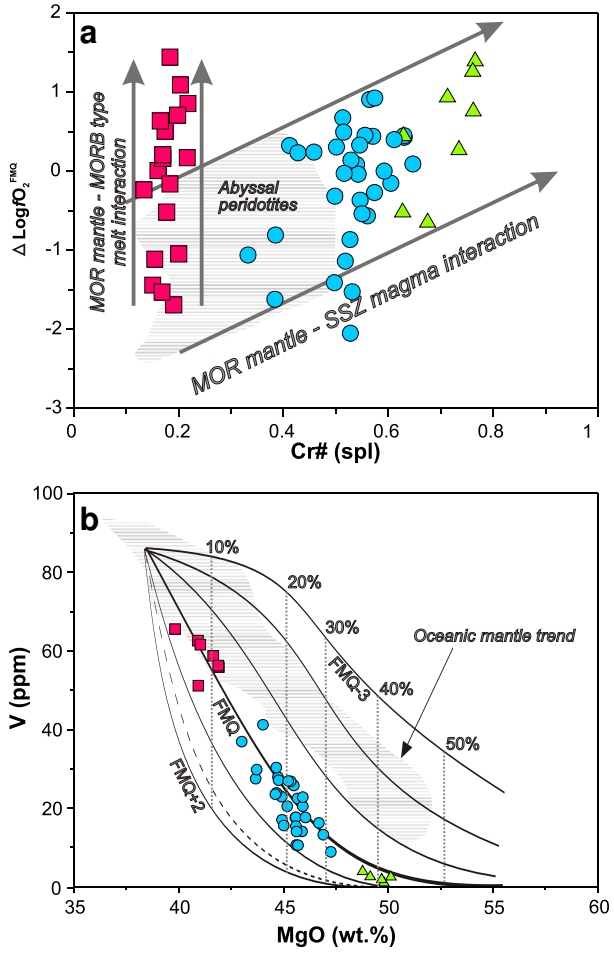

Fig. 12. (a) Plot of $\Delta \log fO_2$ (FMQ) against Cr# of spinel for peridotite samples of the Muğla ophiolite. The field of abyssal peridotites (Parkinson and Pearce, 1998) are also shown for comparison. (b) Melting degrees and oxygen fugacities modeling of peridotite samples of the Muğla ophiolite using V–MgO covariations (after Lee et al., 2003). Partial melting curves are at 1 log unit intervals, spanning fO_2's from FMQ−3 to FMQ+2 (thick solid line represents FMQ). Dashed line represents the unbuffered fractional melting case in which fO_2 is initially prescribed to be FMQ but allowed to evolve with progressive melting in a system closed to O_2 exchange. Dotted vertical lines represent the degree of melt extracted in 10% increments (Lee et al., 2003). Data for oceanic mantle are from Bodinier (1988), Bodinier et al. (1988) and Burnham et al. (1998).

Open-system dynamic melting models have also been applied using Model B as a starting composition and subduction component (compiled from Eiler et al., 2000, 2007) as fluxing material (Fig. 13d). We constructed two models in this case, assuming 0.5% fluxing with 10% melting (Model C) and 0.07% fluxing with 16% melting (Model D). These models describe the REE patterns of the harzburgites and dunites well. Hence, we attribute the physical conditions of these models to second-stage melting and enrichment processes, which may have occurred in a SSZ environment in the genesis of the Muğla peridotites. All these scenarios are also summarized on a La/Yb vs. Yb plot (Fig. 13e). Clinopyroxenes from the cpx-harzburgites and harzburgites are also modeled on a La/Yb vs. Yb diagram (Fig. 13f). On this model, clinopyroxenes of the depleted harzburgites indicate lower degrees of partial melting (~6–12%) with respect to model results using whole rock data (~6–16%). The clinopyroxenes from the depleted harzburgites generally have, in fact, lower Yb contents than the detection limits; therefore, these analyses were not shown on Fig. 13f. Due to the very low concentrations of Yb in the samples and the concentrations being close to the detection limit it is possible that the partial melting may be slightly underestimated and is actually a little more than 20%.

7.5. PGE behavior during partial melting and melt percolation in upper mantle

Major and trace element data of whole rock and minerals from the Muğla peridotites indicate that these rocks were depleted in varying degrees. Therefore, the chemical variations in these peridotites are highly important to understand how PGEs may have behaved during partial melting and melt percolation through the upper mantle. Incompatibility of the PGEs in upper mantle peridotites increase from Os to Pd (Os, Ir, Ru, Rh, Pt, Pd + Re). Therefore, Pt and Pd are highly depleted during partial melting, resulting in the relative enrichment of Os and Ir in the mantle residue (Brenan et al., 2003). The presence of sulfide phases in different stages of mantle melting considerably affects the PGE abundances, as they are highly compatible in sulfides (c.f., Barnes et al., 1997). Varying amounts of sulfide separation from or input into the upper mantle may be an important factor determining the PGE contents of both mantle residues and melts (Bockrath et al., 2004; Rehkamper et al., 1999).

Fig. 9 shows PGE abundances against the Al_2O_3 content, which is indicative of the degree of partial melting. On the same diagram, theoretically calculated depletion trends are also shown. The cpx-harzburgites appear to be depleted ~10–15% with respect to the PM,

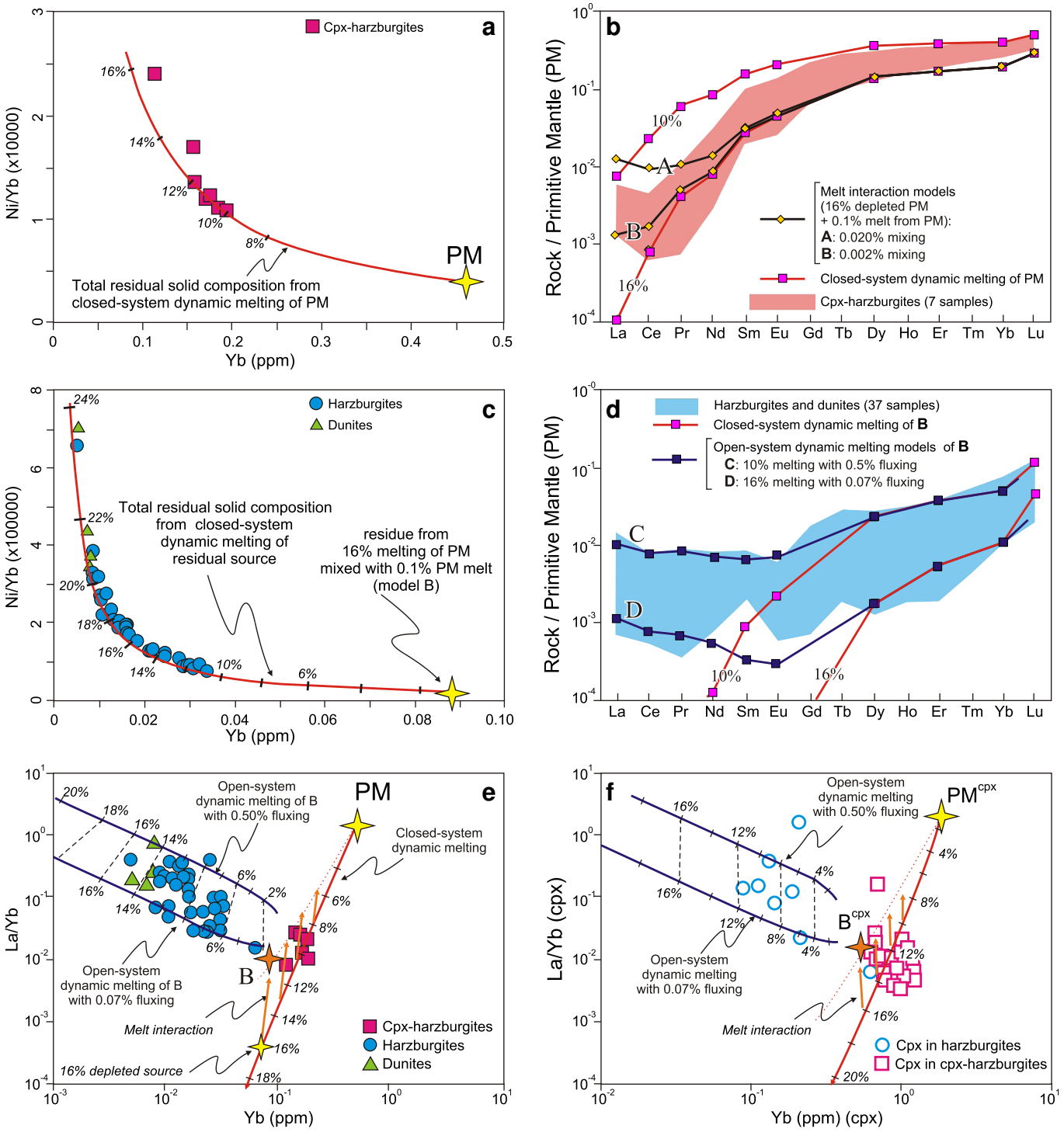

Fig. 13. Trace element melting models for the Muğla peridotites. Closed-system dynamic melting of Primitive Mantle (PM) source (Palme and O'Neill, 2004) is shown on (a) Ni/Yb vs. Ni (ppm) bivariate and (b) PM-normalized multi-element diagrams. Melt interaction model (assuming that 0.5% partial melt from PM interacts with overlying 15% depleted PM) is also shown for 0.015% and 0.002% mixing rates (models A and B). Closed- and open-system dynamic melting of model source B are shown on (c) Ni/Yb vs. Ni (ppm) bivariate and (d) PM-normalized multi-element diagrams. All these models are summarized on La/Yb vs. Yb bivariate diagram for whole rock geochemical data (e) and clinopyroxene LA–ICPMS data (f). Critical value for melt separation is assumed 1% in melting models. Mineral and melt modes are: $Ol_{0.53(-0.06)} + Opx_{0.27(0.28)} + Cpx_{0.27(0.67)} + Spl_{0.03(0.11)}$ (Kinzler, 1997) for first-stage melting models and $Ol_{0.64(-0.06)} + Opx_{0.27(0.28)} + Cpx_{0.09(0.67)} + Spl_{0.02(0.11)}$ for second-stage melting models. The mineral modes for second-stage are calculated for 15% melting. See Appendix 3 for melting parameters.

but their Pd contents with similar depletion degrees are observed above the modeled mantle trend (Fig. 9f). Significant enrichments in Pd are the result of the interaction of melts with the overlying mantle in a MOR environment.

The depleted harzburgite and dunite samples are more depleted with respect to the cpx-harzburgites (20–35% according to their Al_2O_3 contents). However, their PGE concentrations do not follow the melting trend and show instead significant enrichments. This observation is in accordance with the interpretation assuming that the depleted harzburgites and dunites were formed by second-stage partial melting of cpx-harzburgites in a SSZ environment that produced boninitic magmas. In this stage, boninitic melt would be enriched

especially in incompatible PGEs due to the addition of incompatible PGEs derived from the subducted slab. Also, compatible PGEs, such as Os, Ir and Ru, partition to the melt because of the high degrees of hydrous melting of the upper mantle. The interaction of this boninitic melt would enrich the composition of the upper mantle in these elements (Fig. 9). Our analyzed samples reveal the presence of a slightly positive trend from Os to Pd (Fig. 8) that is inconsistent with the nature of the residual mantle material, but can be explained with the inferred scenario discussed above.

7.6. Age of partial melting events from Re–Os constraints

The higher Re concentrations of the samples (up to 1.95 ppb) with respect to PM (0.28, Meisel et al., 2001) cannot be explained by a simple melt extraction and depletion process and may be indicative for secondary Re addition.

Partial melting, serpentinization, sea-floor metamorphism, ophiolite emplacement, and metamorphism are some of the effective processes for Re mobilization (c.f., Batanova et al., 2008). Hence, the most ancient processes causing the Re mobilization could not be older than ~250 Ma, which represents the timing of the opening of the Neo-Tethys. On a Re vs. Al_2O_3 diagram, most of our samples plot above the theoretical melting trend, indicating that the subsequent Re addition might have occurred sometime after 250 Ma. Therefore, we re-calculated the original Re concentrations of the samples according to the method described by Batanova et al. (2008). The minimum ages (T_{RD}) and model ages (T_{MA}), estimated by using these recalculated Re concentrations, vary from negative (future age) to 2895 Ma (Table 4). As proposed by Batanova et al. (2008), the samples tend to have generally ~250, ~400 and ~750 Ma model ages, which may correspond to a series of depletion events related to the opening of the Neo-Tethyan, Rheic, and Proto-Tethyan oceans, respectively. Older ages >1000 Ma may indicate previous depletion events before the opening of Proto-Tethys, most probably related to some melting events in the sub-continental lithospheric mantle of Gondwana. We hence infer that our samples likely represent a heterogeneous upper mantle recording several ancient depletion events.

8. Concluding remarks and regional tectonic implications

On the basis of mineral chemistry, whole-rock major and trace element data, we conclude that the evolution of the Muğla (SW Anatolia) peridotites involved multiple episodes (at least two-staged) of depletion and refertilization. The less depleted samples of the cpx-harzburgite may represent the restite of low-degree, first-stage partial melting. The depleted harzburgite and dunite rock units formed, however, during the second-stage partial melting and melt–peridotite interaction of a previously depleted mantle (cpx-harzburgite) in SSZ setting. Trace element compositions of the cpx-harzburgites can be modeled by up to ~10–16% dynamic melting of a PM-like mantle source. Trace element abundances of the depleted harzburgites and dunites, on the other hand, can be reproduced by ~10–16% open-system melting of an already depleted (~16%) mantle.

These melting models are also supported by our PGE data. Chondrite-normalized PGE abundances of the analyzed samples do not show negative slope from Os to Pd that should be expected for partial melting residuals. This implies redistribution of PGEs, especially incompatible PGEs, during melting in the mantle wedge that also caused the Re redistribution in the peridotites. The wide range of Re-depletion ages obtained from the samples likely corresponds to a series of tectonic events related to the opening and closure of Neo-Tethys.

The effects of two-stage melting events, deduced from the geochemical data, can also be supported by the Re–Os systematics. The record of these melting events, related to (1) the opening of Neo-Tethys via seafloor spreading (~250 Ma) and (2) the closure of Neo-Tethys by intra-oceanic subduction (~90 Ma), can be traced in both rock groups. During first-stage depletion, the Re budget of the PM was depleted at ~250 Ma. The remaining ^{187}Re contents in the restite decayed to ^{187}Os until the second melting event that occurred at ~90 Ma. During the second-stage depletion, the mantle residue became highly depleted. Therefore, since ~90 Ma, little ^{187}Re has been decaying to ^{187}Os. This explains the slightly lower $^{187}Os/^{188}Os$ of the second-stage melting residue of the depleted harzburgites than those of the first-stage partial melting residue, the cpx-harzburgites. The model ages of ~250 Ma, ~400 Ma and ~750 Ma that we traced in the Muğla peridotites may correspond to those tectonic events related to the geodynamic evolution of the Neo-Tethyan, Rheic, and Proto-Tethyan oceans, respectively. The >1000 Ma model ages we obtained can be interpreted as a result of a more ancient melting event before the Proto-Tethyan evolution.

Acknowledgments

This study is based in part on the PhD thesis of I. Uysal in Karadeniz Technical University, Turkey. The financial background of this study was made available by a grant from the Scientific Research Foundation of Karadeniz Technical University (#2005.112.005.05) and by the Socrates/Erasmus and DAAD (German Academic Exchange Services) scholarships to I. Uysal (2004–2005). The constructive comments by Olivier Alard and Tomoaki Morishita were most helpful to improve an earlier version of the manuscript. We are indebted to Haydar Aygün for his help in the field. Special thanks are due to S. Heidrich for her help during the electron-microprobe analyses and to Peter Stutz for the preparation of polished sections. Ali Polat, G. Nelson Eby, and an anonymous reviewer are greatly acknowledged for their thorough and insightful comments, which significantly improved the manuscript.

Appendix A. Supplementary data

Supplementary data to this article can be found online at doi:10.1016/j.lithos.2011.11.009.

References

Acken, D., Becker, H., Walker, R.J., 2008. Refertilization of Jurassic oceanic peridotites from the Tethys Ocean — implications for the Re–Os systematics of the upper mantle. Earth and Planetary Science Letters 268, 171–181.

Adam, J., Green, T., 2006. Trace element partitioning between mica- and amphibole-bearing garnet lherzolite and hydrous basanitic melt: 1. Experimental results and the investigation of controls on partitioning behavior. Contributions to Mineralogy and Petrology 152, 1–17.

Alard, O., Griffin, W.L., Lorand, J.P., Jackson, S.E., O'Reilly, S.Y., 2000. Non-chondritic distribution of the highly siderophile elements in mantle sulphides. Nature 407, 891–894.

Alard, O., Griffin, W.L., Pearson, N.J., Lorand, J.P., O'Reily, S.Y., 2002. New insights into the Re–Os systematics of sub-continental lithospheric mantle from in situ analysis of sulphides. Earth and Planetary Science Letters 203, 651–663.

Alard, O., Luguet, A., Pearson, N.J., Griffin, W.L., Lorand, J.P., Gannoun, A., Burton, K.W., O'Reilly, S.Y., 2005. In situ Os isotopes in abyssal peridotites bridge the isotopic gap between MORBs and their source mantle. Nature 436, 1005–1008.

Alçiçek, M.C., 2007. Tectonic development of an orogen-top rift recorded by its terrestrial sedimentation pattern: the Neogene Eşen Basin of southwestern Anatolia, Turkey. Sedimentary Geology 200, 117–140.

Aldanmaz, E., Köprübaşı, N., 2006. Platinum-group-element systematics of peridotites from ophiolite complexes of Northwest Anatolia, Turkey: implications for mantle metasomatism by melt percolation in a supra-subduction zone environment. International Geology Review 48, 420–442.

Aldanmaz, E., Schmidt, M.W., Gourgaud, A., Meisel, T., 2009. Mid-ocean ridge and supra-subduction geochemical signatures in spinel–peridotites from the Neotethyan ophiolites in SW Turkey: implications for upper mantle melting processes. Lithos 113, 691–708.

Arai, S., 1992. Chemistry of chromian spinel in volcanic rocks as a potential guide to magma chemistry. Mineralogical Magazine 56, 173–184.

Arai, S., 1994. Characterization of spinel peridotites by olivine–spinel compositional relationships, review and interpretation. Chemical Geology 113, 191–204.

Arculus, R.J., 1994. Aspects of magma genesis in arcs. Lithos 33, 189–208.

Ballhaus, C., Berry, R.F., Green, D.H., 1991. High pressure experimental calibration of the olivine–orthopyroxene–spinel oxygen barometer, implications for the oxidation of the mantle. Contributions to Mineralogy and Petrology 107, 27–40.
Ballhaus, C., Bockrath, C., Wohlgemuth-Ueberwasser, C., Laurenz, V., Bernd, J., 2006. Fractionation of the noble metals by physical processes. Contributions to Mineralogy and Petrology 152, 667–684.
Barnes, S.J., Makovicky, M., Mackovicky, E., Karup-Möller, S., 1997. Partition coefficients for Ni, Cu, Pd, Pt, Rh and Ir between monosulfide solid solution and sulfide liquid and the formation of compositionally zones Ni–Cu sulfide bodies by fractional crystallization of sulfide liquid. Canadian Journal of Earth Sciences 34, 366–374.
Barth, M.G., Mason, P.D., Davies, G.R., Dijkstra, A.H., Drury, M.R., 2003. Geochemistry of the Othris Ophiolite, Greece: evidence for refertilization? Journal of Petrology 44, 1759–1785.
Batanova, V.G., Brügmann, G.E., Bazylev, B.A., Sobolev, A.V., Kamenetsky, V.S., Hofmann, A.W., 2008. Platinum-group element abundances and Os isotope composition of mantle peridotites from the Mamonia complex, Cyprus. Chemical Geology 248, 195–212.
Bockrath, C., Ballhaus, C., Holzheid, A., 2004. Stabilities of laurite RuS_2 and monosulfide liquid solution at magmatic temperature. Chemical Geology 208, 265–271.
Bodinier, J.L., 1988. Geochemistry and petrogenesis of the Lanzo Peridotite Body, Western Alps. Tectonophysics 149, 67–88.
Bodinier, J.L., Godard, M., 2003. Orogenic, ophiolitic, and abyssal peridotites, in the mantle and core. In: Carlson, R.W. (Ed.), Treatise on Geochemistry v. 2. Elsevier-Pergamon, Oxford. ISBN 0-08-043751-6.
Bodinier, J.L., Dupuy, C., Dostal, J., 1988. Geochemistry and petrogenesis of Eastern Pyrenean peridotites. Geochimica et Cosmochimica Acta 52, 2893–2907.
Bodinier, J.L., Garrido, C.J., Chanefo, I., Bruguier, O., Gervilla, F., 2008. Origin of pyroxenite–peridotite veined mantle by refertilization reactions: evidence from the Ronda peridotite (southern Spain). Journal of Petrology 49, 999–1025.
Bonatti, E., Michael, P.J., 1989. Mantle peridotites from continental rifts to ocean basins to subduction zones. Earth and Planetary Science Letters 91, 297–311.
Brenan, J.M., McDonough, W.F., Dalpe, C., 2003. Experimental constraints on the partitioning of rhenium and some platinum-group elements between olivine and silicate melt. Earth and Planetary Science Letters 212, 135–150.
Burnham, O.M., Rogers, N.W., Pearson, D.G., van Calsteren, P.W., Hawkesworth, C.J., 1998. The petrogenesis of the eastern Pyrenean peridotites: an integrated study of their whole-rock geochemistry and Re–Os isotope composition. Geochimica et Cosmochimica Acta 62, 2293–2310.
Choi, S.H., Shervais, J.W., Mukasa, S.B., 2008. Supra-subduction and abyssal mantle peridotites of the Coast range ophiolite, California. Contributions to Mineralogy and Petrology 156, 551–576.
Collins, A.S., Robertson, A.H.F., 2003. Kinematic evidence for Late Mesozoic–Miocene emplacement of the Lycian Allochthon over the Western Anatolide Belt, SW Turkey. Geological Journal 38, 295–310.
Dick, H.J.B., Bullen, T., 1984. Chromium spinel as a petrogenetic indicator in abyssal and Alpine-type peridotites and spatially associated lavas. Contributions to Mineralogy and Petrology 86, 54–76.
Dick, H.J.B., Natland, J.H., 1996. Late stage melt evolution and transport in the shallow mantle beneath the East Pacific Rise. Deep See Drilling Project, Initial Reports 147, 103–134.
Dilek, Y., Furnes, H., 2009. Structure and geochemistry of Tethyan ophiolites and their petrogenesis in subduction rollback systems. Lithos 113, 1–20.
Dilek, Y., Furnes, H., 2011. Ophiolite genesis and global tectonics: geochemical and tectonic fingerprinting of ancient oceanic lithosphere. The Geological Society of America Bulletin 123, 387–411.
Dilek, Y., Morishita, T., 2009. Melt migration and upper mantle evolution during incipient arc construction: Jurassic Eastern Mirdita ophiolite, Albania. Island Arc 18, 551–554.
Dilek, Y., Rowland, J.C., 1993. Evolution of a conjugate passive margin pair in Mesozoic southern Turkey. Tectonics 12, 954–970.
Dilek, Y., Thy, P., 2006. Age and petrogenesis of plagiogranite intrusions in the Ankara Melange, Central Turkey. Island Arc 15, 44–57.
Dilek, Y., Thy, P., Hacker, B., Grundvig, S., 1999. Structure and petrology of Tauride ophiolites and mafic dike intrusions (Turkey): implications for the Neo-Tethyan Ocean. Bulletin of the Geological Society of America 111, 1192–1216.
Dilek, Y., Moores, E.M., Elthon, D., Nicolas, A., 2000. Ophiolites and oceanic crust: new insights from field studies and the Ocean Drilling Program. Geological Society of America Special Paper 349, 552 ISBN 0-8137-2349-3.
Eiler, J.M., Crawford, A., Elliott, T., Farley, K.A., Valley, J.W., Stolper, E.M., 2000. Oxygen isotope geochemistry of oceanic-arc lavas. Journal of Petrology 41, 229–256.
Eiler, J.M., Schiano, P., Valley, J.W., Kita, N.T., Stolper, E.M., 2007. Oxygen-isotope and trace element constraints on the origins of silica-rich melts in the subarc mantle. Geochemistry, Geophysics, Geosystems 8, Q09012.
Gaetani, G.A., Grove, T.L., 1998. The influence of water on melting of mantle peridotite. Contributions to Mineralogy and Petrology 131, 323–346.
Garuti, G., Fershtater, G., Bea, F., Montero, P., Pushkarev, E.V., Zaccarini, F., 1997. Platinum-group elements as petrological indicators in mafic–ultramafic complexes of the central and Southern Urals, preliminary results. Tectonophysics 276, 181–194.
Gervilla, F., Proenza, J.A., Frei, J.M., Gonzales-Jimenez, C.J., Garrido, J.C., Melgajero, A., Meibom, A., Diaz-Martinez, R., Lavaut, W., 2005. Distribution of platinum-group elements and Os isotopes in chromite ores from Mayari-Baracoa (eastern Cuba). Contribution to Mineralogy and Petrology 150, 589–607.
Ghazi, J.M., Moazzen, M., Rahgoshay, M., Moghada, H.S., 2010. Mineral chemical composition and geodynamic significance of peridotites from Nain ophiolite, central Iran. Journal of Geodynamics 49, 261–270.
Ghiorso, M.S., Hirschmann, M.M., Reiners, P.W., Kress III, V.C., 2002. The pMELTS: a revision of MELTS aimed at improving calculation of phase relations and major element partitioning involved in partial melting of the mantle at pressures up to 3 GPa. Geochemistry Geophysics Geosystems 3 (5). doi:10.1029/2001GC000217.
Godard, M., Lagabrielle, Y., Alard, O., Harvey, J., 2008. Geochemistry of the highly depleted peridotites drilled at ODP Sites 1272 and 1274 (Fifteen-Twenty Fracture Zone, Mid-Atlantic Ridge): implications for mantle dynamics beneath a slow spreading ridge. Earth and Planetary Science Letters 267, 410–425.
Hanghoj, K., Kelemen, P.B., Hassler, D., Godard, M., 2010. Composition and genesis of depleted mantle peridotites from theWadiTayin Massif, Oman Ophiolite; major and trace element geochemistry, and Os isotope and PGE systematics. Journal of Petrology 51, 201–227.
Hart, S.R., Zindler, A., 1986. In search of a bulk-Earth composition. Chemical Geology 57, 247–267.
Hebert, R., Adamson, A.C., Komor, S.C., 1990. Metamorphic petrology of ODP 109, Hole 670A serpentinized peridotites: serpentinization processes at a slow spreading ridge environment. In: Detrick, R., Honnorez, J., Bryan, W.B., Juteau, T. (Eds.), Proceedings of the ODP, Sci. Results 106/109. College Station, Texas, pp. 103–115.
Hellebrand, E., Snow, J.E., Dick, H.J.B., Hofmann, A.W., 2001. Coupled major and trace elements as indicators of the extent of melting in mid-ocean-ridge peridotites. Nature 410, 677–681.
Hellebrand, E., Snow, J.E., Mühe, R., 2002. Mantle melting beneath Gakkel Ridge (Arctic Ocean): abyssal peridotite spinel compositions. Chemical Geology 182, 227–235.
Ishii, T., Robinson, P.T., Maekawa, H., Fiske, R., 1992. Petrological studies of peridotites from diapiric serpentinite seamounts in the Izu–Ogasawara–Mariana Forearc, Leg 125. In: Fryer, O., Pearce, J.A., Stokking, L.B. (Eds.), Proceedings of the Ocean Drilling Program, Scientific Results, 125. Ocean Drilling Program, College Station, TX, pp. 445–485.
Jagoutz, E., Palme, H., Blum, H., Cendales, M., Dreibus, G., Spettel, B., Lorenz, V., Wanke, H., 1979. The abundances of major, minor and trace elements in the Earth's mantle as derived from primitive ultramafic nodules. Proceedings of 10th Lunar Planetary Science Conference. Geochimica et Cosmochimica Acta Supplements 10, 2031–2051.
Johnson, K.T.M., Dick, H.J.B., 1992. Open system melting and temporal and spatial variation of peridotite and basalt at the Atlantis II fracture zone. Journal of Geophysical Research 97, 9219–9241.
Johnson, K.T.M., Dick, H.J.B., Shimizu, N., 1990. Melting in the oceanic upper mantle: an ion microprobe study of diopsides in abyssal peridotites. Journal of Geophysical Research 95, 2661–2678.
Kelemen, P.B., Dick, H.J.B., Quick, J.E., 1992. Formation of harzburgite by pervasive melt–rock reaction in the upper Mantle. Nature 358, 635–641.
Kinzler, 1997. Melting of mantle peridotite at pressures approaching the spinel to garnet transition: application to mid-ocean ridge basalt petrogenesis. Journal of Geophysical Research 102, 853–874.
Lapierre, H., Samper, A., Bosch, D., Maury, R.C., Bechennec, F., Cotten, J., Demant, A., Brunet, P., Keller, F., Marcoux, J., 2004. The Tethyan plume: geochemical diversity of Middle Permian basalts from the Oman rifted margin. Lithos 74, 167–198.
Lee, C.-T.A., Brandon, A.D., Norman, M., 2003. Vanadium in peridotites as a proxy of Paleo-fO_2 during partial melting, prospects, limitations and implications. Geochimica et Cosmochimica Acta 67, 3045–3064.
Lorand, J.P., Alard, O., 2001. Platinum-group element abundances in the upper mantle, new constraints from in situ and whole-rock analyses of massif central xenoliths (France). Geochimica et Cosmochimica Acta 65, 2789–2806.
Lorand, J.P., Luguet, A., Alard, O., Bezos, A., Meisel, T., 2008. Abundance and distribution of platinum-group elements in orogenic lherzolites; a case study in a Fontete Rouge lherzolite (French Pyrénées). Chemical Geology 248, 174–194.
Luguet, A., Alard, O., Lorand, J.P., Pearson, N.J., Ryan, C., O'Reilly, S.Y., 2001. Laser-ablation microprobe (LAM)–ICPMS unravels the highly siderophile element geochemistry of the oceanic mantle. Earth and Planetary Science Letters 189, 285–294.
Luguet, A., Lorand, J.P., Seyler, M., 2003. A coupled study of sulphide petrology and highly siderophile element geochemistry in abyssal peridotites from the Kane Fracture Zone (Mark area, Mid-Atlantic Ridge). Geochimica et Cosmochimica Acta 67, 1553–1570.
Marchesi, C., Garrido, C.J., Godard, M., Proenza, J.A., Gervilla, F., Blanco-Moreno, J., 2006. Petrogenesis of highly depleted peridotites and gabbroic rocks from the Mayari-Baracoa ophiolitic belt (Eastern Cuba). Contributions to Mineralogy and Petrology 151, 717–736.
McDonough, W.F., Sun, S.S., 1995. The composition of the earth. Chemical Geology 120, 223–253.
Meisel, T., Moser, J., Wegscheider, W., 2001. Recognizing heterogeneous distribution of platinum group elements (PGE) in geological materials by means of the Re–Os isotope system. Fresenius Journal of Analytical Chemistry 370, 566–572.
Meisel, T., Fellner, N., Moser, J., 2003. A simple procedure for the determination of platinum group elements and rhenium (Ru, Rh, Pd, Re, Os, Ir and Pt) using ID-ICP-MS with an inexpensive on-line matrix separation in geological and environmental materials. Journal of Analitical Atomic Spectrometry 18, 720–726.
Melcher, F., Meisel, T., 2004. A metamorphosed Early Cambrian crust–mantle transition in the Eastern Alps, Austria. Journal of Petrology 45, 1689–1723.
Nell, J., Wood, B.J., 1991. High-temperature electrical measurements and thermodynamic properties of Fe_3O_4–$FeCr_2O_4$–$MgCr_2O_4$–$FeAl_2O_4$ spinels. American Mineralogist 76, 405–426.
Nicolas, A., Prinzhofer, A., 1983. Cumulative or residual origin for the transition zone in ophiolites: structural evidence. Journal of Petrology 24, 188–206.
Niu, Y., 2004. Bulk-rock major and trace element composition of abyssal peridotites, implications for mantle melting, melt extraction and post-melting processes beneath Mid-ocean Ridges. Journal of Petrology 45, 2423–2458.
Niu, Y., Langmuir, C.H., Kinzler, R.J., 1997. The origin of abyssal peridotites: a new perspective. Earth and Planetary Science Letters 152, 251–265.
Okamura, H., Arai, S., Kim, Y.U., 2006. Petrology of forearc peridotite from the Hahajima Seamount, the Izu–Bonin arc, with special reference to chemical characteristics of chromian spinel. Mineralogical Magazine 70, 15–26.

Okay, İ.A., Tansel, İ., Tüysüz, O., 2001. Obduction, subduction and collision as reflected in the Upper Cretaceous–Lower Tertiary sedimentary record of western Turkey. Geological Magazine 138, 117–142.
Ottley, C.J., Pearson, D.G., Irvine, G.J., 2003. A routine method for the dissolution of geological samples for the analysis of REE and trace elements via ICP–MS. In: Holland, J.G., Taner, S.D. (Eds.), Plasma Source Mass Spectrometry, Applications and Emerging Technologies: The Royal Society of Chemistry, pp. 221–230.
Paliulionyte, V., Meisel, T., Ramminger, P., Kettisch, P., 2006. High pressure asher digestion and an Isotope Dilution–ICP-MS method for the determination of platinum-group element concentrations in chromitite reference materials CHR-Bkg, GAN Pt-1 and HHH. Geostandards and Geoanalytical Research 30, 87–96.
Palme, H., O'Neill, H.St.C., 2004. Cosmochemical estimates of mantle composition. In: Holland, H.D., Turrekian, K.K. (Eds.), Treatise on Geochem, vol. 2. Elsevier, Amsterdam, pp. 1–38.
Parkinson, I.J., Arculus, R.J., 1999. The redox state of subduction zones, insides from arc-peridotites. Chemical Geology 160, 409–423.
Parkinson, I.J., Pearce, J.A., 1998. Peridotites from the Izu–Bonin–Mariana Forearc (ODP Leg 125), evidence for mantle melting and melt–mantle interaction in a supra-subduction zone setting. Journal of Petrology 39, 1577–1618.
Parkinson, I.J., Arculus, R.J., Eggins, S.M., 2003. Peridotite xenoliths from Grenada, Lesser Antilles Island Arcs. Contributions to Mineralogy and Petrology 146, 241–262.
Pearce, J.A., Barker, P.F., Edwards, S.J., Parkinson, I.J., Leat, P.T., 2000. Geochemistry and tectonic significance of peridotites from the South Sandwich Arc-basin Systems, South Atlantic. Contributions to Mineralogy and Petrology 139, 36–53.
Poisson, A., Yağmurlu, F., Bozcu, M., Şentürk, M., 2003. New insights on the tectonic setting and evolution around the apex of the Isparta Angle (SW Turkey). Geological Journal 38, 257–282.
Potts, P.J., Tindle, A.G., Webb, P.C., 1992. Geochemical Reference Materials Compositions, Rocks, Minerals, Sediments, Soils, Carbonates, Refractories and Ores Used in Research and Industry. Whittles Publishing, Caithness.
Pouchou, J.L., Pichoir, F., 1984. A new model for quantitative X-ray microanalysis. Application to the analysis of homogeneous samples. La Recherche Aerospatiale (English Edition) 3, 13–38.
Rampone, E., Piccardo, G.B., Hofman, A.W., 2008. Multi-stage melt–rock interaction in the Mt. Maggiore (Corsica, France) ophiolitic peridotites: microstructural and geochemical evidence. Contributions to Mineralogy and Petrology 156, 453–475.
Rehkamper, M., Halliday, A.N., Barford, D., Fitton, J.G., Zipfel, J., Takazawa, E., 1999. Non-chondritic platinum-group element ratios in oceanic mantle lithosphere, petrogenetic signature of melt percolation? Earth and Planetary Science Letters 172, 65–81.
Robertson, A.H.F., 2002. Overview of the genesis and emplacement of mesozoic ophiolites in the Eastern Mediterranean Tethyan Region. Lithos 65, 1–67.
Şenel, M., 1997. Geological Maps of Turkey in 1:100,000 scale: Fethiye L8 sheet. Mineral Research and Exploration Directorate of Turkey, Ankara. 22 pp.
Seyler, M., Toplis, M.J., Lorand, J.P., Luguet, A., Cannat, M., 2001. Clinopyroxene microtextures reveal incompletely extracted melts in abyssal peridotites. Geology 29, 155–158.
Shirey, S.B., Walker, R.J., 1998. The Re–Os isotope system in cosmochemistry and high-temperature geochemistry. Annual Review of Earth and Planetary Sciences 26, 423–500.
Smoliar, M.I., Walker, R.J., Morgan, J.W., 1996. Re–Os ages of Groups IIA, IIIA, IVA, and IVB iron meteorites. Science 271, 1099–1102.
Snow, J.E., Dick, H.J.B., 1995. Pervasive magnesium loss by marine weathering of peridotite. Geochimica et Cosmochimica Acta 59, 4219–4235.
Takazawa, E., Frey, F.A., Shimizu, N., Obata, M., 2000. Whole rock compositional variations in an upper mantle peridotite (Horoman, Hokkaido, Japan): are they consistent with a partial melting process? Geochemica et Cosmochimica Acta 64, 695–716.
Thuizat, R., Whitechurch, H., Montigny, R., Juteau, T., 1981. K–Ar dating of some infra-ophiolitic metamorphic soles from the Eastern Mediterranean: new evidence for oceanic thrustings before obduction. Earth and Planetary Science Letters 52, 302–310.
Tiepolo, M., Bottazzi, P., Palenzona, M., Vannucci, R., 2003. A laser probe coupled with ICP-double-focusing sector-field mass spectrometer for ın situ analysis of geological sampled and U–Pb dating of zircon. The Canadian Mineralogist 41, 259–272.
Uysal, I., 2007. Petrology of upper mantle peridotite and ophiolitic chromitites from the Muğla (SW-Turkey): implications from mineral chemistry, major–trace–rare earth elements (REE)–platinum-group elements (PGE) geochemistry, PGE mineralogy and Re–Os isotope systematics. PhD Thesis, Karadeniz Technical University, Trabzon, Turkey, 449 pp.
Uysal, I., Sadıklar, M.B., Tarkian, M., Karslı, O., Aydın, F., 2005. Mineralogy and composition of the chromitites and their platinum-group minerals from Ortaca (Muğla-SW Turkey): evidence for ophiolitic chromitite genesis. Mineralogy and Petrology 83, 219–242.
Uysal, I., Kaliwoda, M., Karslı, O., Tarkian, M., Sadıklar, M.B., Ottley, C.J., 2007. Compositional variations in whole rock and coexisting phases with partial melting and melt–peridotite interaction in an upper mantle section from the Ortaca Area, Southwestern Turkey. Canadian Mineralogist 45, 1471–1493.
Uysal, I., Tarkian, M., Sadiklar, M.B., Zaccarini, F., Meisel, T., Garuti, G., Heidrich, S., 2009. Petrology of high-Cr and high-Al ophiolitic chromitites from the Muğla, SW Turkey: implications from composition of chromite, solid inclusions of platinum-group mineral (PGM), silicate, and base-metal mineral (BMM), and Os-isotope geochemistry. Contributions to Mineralogy and Petrology 158, 659–674.
Walker, R.J., Carlson, R.W., Shirey, S.B., Boyd, F.R., 1989. Os, Sr, Nd, and Pb isotope systematics of southern African peridotite xenoliths: implications for the chemical evolution of subcontinental mantle. Geochimica et Cosmochimica Acta 53, 1583–1595.
Zhou, M.-F., Robinson, P.T., Malpas, J., Edwards, S.J., Qi, L., 2005. REE and PGE geochemical constraints on the formation of dunite in the Luobusa ophiolite, Southern Tibet. Journal of Petrology 46, 615–639.